University of Stavanger

Faculty of Science and Technology

MASTER'S THESIS

Study program/Specialization: **Marine and Offshore Technology**	Spring semester, 2021 Open
Writer: **Magnus Aske Mjåtveit**	*Magnus A. Mjåtveit* .... (Writer's signature)

Faculty supervisor: **Prof. Muk Chen Ong**

Co-supervisor(s): **Mr. Hui Cheng**

Thesis title:

    Numerical study of two typical Norwegian gravity-based fish cages with different cage shapes and weights

Credits (ECTS): 30

Key words: **Circular cage** **Squared cage** **Drag force** **Cultivation volume**	Pages: 65 + enclosure: 0 Stavanger, June 15. 2021

NUMERICAL STUDY OF TWO TYPICAL NORWEGIAN GRAVITY-BASED FISH CAGES WITH DIFFERENT CAGE SHAPES AND WEIGHTS
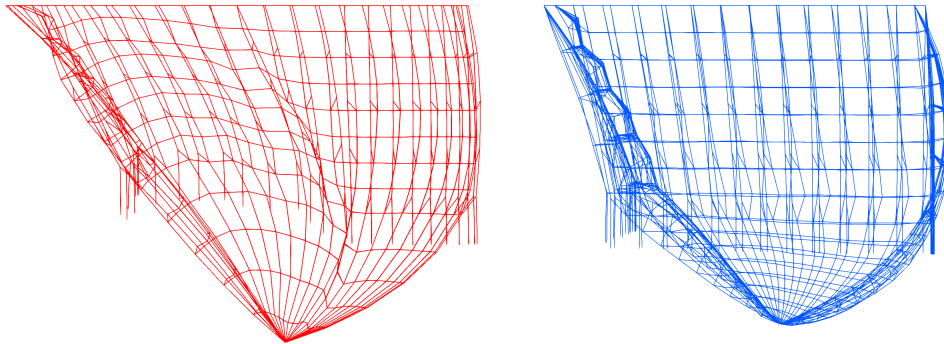
Author: Magnus Aske Mjåtveit

Supervisor: Prof. Muk Chen Ong

Co-supervisor: Mr. Hui Cheng

University of Stavanger

Faculty of Science and Technology

Department of Mechanical and Structural Engineering and Material Science

Master of Science Thesis, Spring 2021

Abstract

Fish cages usually have net deformation in marine environments, and this deformation can reduce the cultivation volume of the fish cage and thus reduce the fish welfare. Hence, it is necessary to understand the structural responses of fish cages under various environmental conditions. In the present thesis, two hydrodynamic models, *i.e.*, Morison model and Screen model, are implemented into a general finite element (FE) solver Code_Aster as a new module for dynamic analyses of fish cages.

Two typical Norwegian fish cage models with circular and squared shapes are developed in the present study and are employed to compare their structural responses and net deformation. The comparative study of the two fish cages is carried out with different dimensions (*i.e.*, circumferences and design heights), weights and current velocities. Correspondingly, the numerical results from the study are collated and investigated using Python scripts.

Firstly, the drag forces of the two fish cages are compared. The primary difference in drag force is caused by the shapes of the two fish cages, where the circular fish cage experiences a larger cage deformation for strong current velocities than the squared cage. The numerical results indicate that the squared cage induces a larger drag force than the circular cage, when both cages have the same dimensions, weights and current velocities.

Secondly, the total cultivation volume and the volume factor are calculated and compared. When $U < 0.4$ m/s, the circular cage has a larger cultivation volume than the squared cage for the same dimensions and weight. Overall, the squared cage has a greater volume factor than the circular cage for different dimensions, weight and current velocities. The squared fish cage produces a larger cultivation volume per netting area and volume factor per netting area than the circular fish cage.

Lastly, the fish cage height and cross-section area of the two fish cages are compared. With the same dimensions and weight, the circular cage has a larger fish cage height than the squared cage when $U < 0.4$ m/s. The circular fish cage has a larger cross-section area than the squared cage when $U < 0.5$ m/s, given the same dimensions and weight.

Acknowledgement

Firstly, I would like to thank my supervisor, Prof. Muk Chen Ong, for introducing me to aquaculture and giving me motivation to pursue future work in the field. Throughout my thesis, he has given me mentoring and exceptional guiding.

Secondly, I would extend my gratitude to Mr. Hui Cheng, for his inspiration and consistent academic feedback regarding writing and programming. His expertise and knowledge greatly inspired me.

Table of Contents

List of Figures

List of Tables

1. Introduction

Aquaculture is one of the most rapid growing industries for food production worldwide. As the global market for fish farming is on the rise, a demand for more fish is needed for the populating world. In 2016, aquaculture was estimated to comprise of 47 % of the total fish production (SOFIA, 2018). One way of meeting the demand is to expand the fish cages, which increases the cultivation volume and the possibility of farming more fish. This expansion comprises of increasing the circumference and/or design height of the fish cage, where the circumference of Norwegian fish cages can be as large as 157 m (Føre et al., 2018).

One challenge in Norwegian aquaculture is the escape of fish. While the escape may sound harmless, it causes mutations of deceases in the fish wildlife. Typical Norwegian fish farms breeds salmon, which, if they escape from their cage, may disrupt gene pools of natural salmons. Føre and Thorvaldsen (2021), performed a quantitative analysis of the escape of Atlantic salmon (*Salmo salar*) and rainbow trout (*Oncorhynchus mykiss*) from Norwegian fish farms. Almost 2 million fish escaped over a nine-year period from 2010 to 2018, registered by the Norwegian Directorate of Fisheries. The main reason for escapes in sea-based fish farms is due to holes in the nets, where half of the escapes through the holes are caused by the weight system applied to the fish cage. Figure 1 shows the typical contributions of fish escape in sea-based fish farms.

In general, different types of weight systems can be applied to a fish cage, in order to mitigate net deformation when fish cages are subjected to strong current velocities. The most common weight systems are simple weights (sinkers attached to floating collars using side ropes), suspension collars (sustaining the shape at the bottom of main netting) and a single weight attached to the bottom net. In practice, the selection of supporting weights depends on net material, cage shape and environmental conditions.

Weight system

47%

22%

Main components

17%

Auxiliary equipment

8%

External factors

6%

Inconclusive
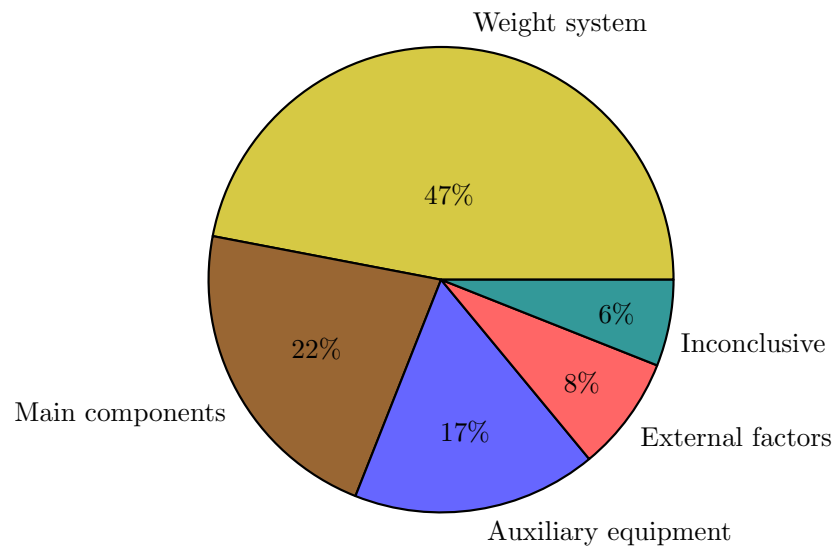
Figure 1. Main contributing factors for escape of Atlantic salmon and rainbow trout in Norwegian fish farms from 2010 to 2018 (Føre and Thorvaldsen, 2021).

1.1. Environmental conditions and fish farm assembly

Even though aquaculture has resolved many aspects regarding fish disease, utilizing natural resources, economic growth and employment, there are concerns related to negative environmental impacts of the industry (Bjørkan and Eilertsen, 2020). In order to minimize environmental impacts, such as erosion of the bottom sediment, repositioning of fish farms further offshore is becoming an inevitable trend. When deployed in such an environment, the fish farm tends to be exposed to the tidal current instead of a constant current (Bi and Xu, 2018). For salmon aquaculture, 0.2 to 0.5 m/s is the optimal current velocity and 0.75 m/s is the maximum current velocity which is recommended (Cardia and Lovatelli, 2015). When a fish cage is exposed in an open-sea area, strong waves can cause displacement and deformation, which may reduce the functionality of the fish cage (Huang et al., 2016). Currently, the concept of designing fish cages for offshore environment is still in its infancy. Hence, it is important to derive an optimum cage design concept in order to sustain durability (Shainee et al., 2013).

Fish cages are usually assembled with mooring lines, anchors, buoys and frame cables. Figure 2 shows the assembly of typical elements supporting a fish cage. The fish cage is constructed with a floating collar made of high-density polyethene (HDPE). In practice, the

floating collar provides a subsequent buoyancy force which sustain the fish cage floating. In addition to the logical buoyancy force generated by the floating collar, supplementary buoys are implemented to support mooring lines and are connected with a frame cable. The floating collar provides a foundation for attachment of the main net and ropes. The main net usually consists of multiple nets to prevent fish from escaping. Typical fish cages are installed with polymer nettings and nylon (or polyamide) ropes (Cardia and Lovatelli, 2015).
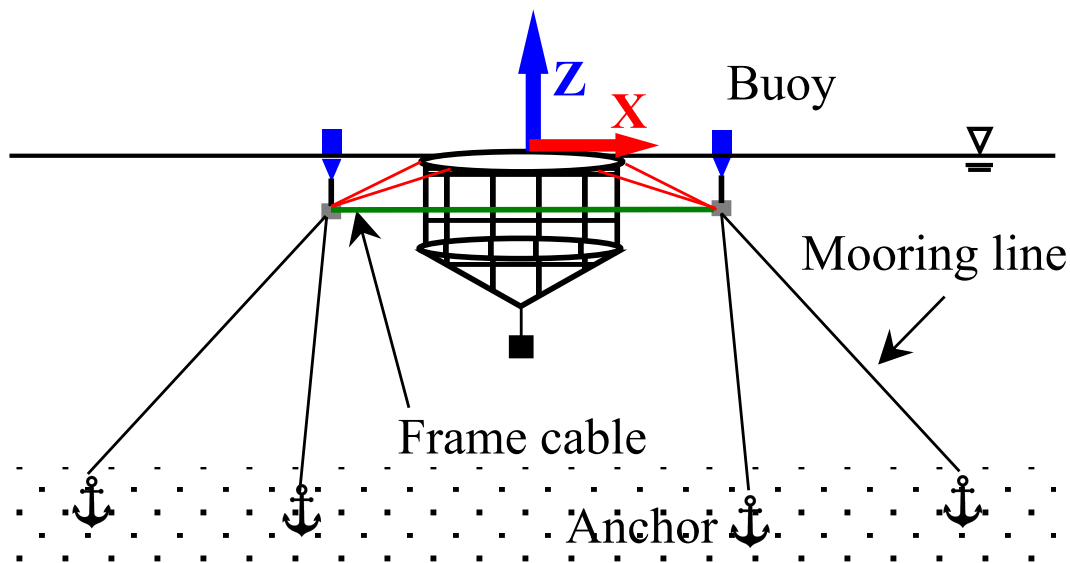
Figure 2. Supporting elements adjacent a fish cage.

Throughout the last decades, a number of researchers have investigated hydrodynamic forces and cage deformations of different cage shapes and weight systems. Théret (1993), successfully created a software for calculating the hydrodynamic forces and the corresponding shapes of a trawl exposed to a constant flow velocity. A Finite Element Method (FEM) was proposed by Tsukrov et al. (2003) to investigate the structural responses of net panels subjected to environmental loading. Endresen and Klebert (2020), compared experimental and simulated loads and responses on flexible conical and cylindrical fish cages, where the numerical results underestimated the drag forces. Chen et al. (2021), investigated the volume reduction for cylindrical and elliptical fish cages

with different weight configurations. They found that heavier bottom weights mitigated the net volume reduction and increased the drag force under large current velocities.

In order to predict the hydrodynamic forces acting on fish cages, researchers did considerable work to find the dominant parameters. Balash et al. (2009) concluded from experiments that drag coefficients for nets and cylinders are equivalent, modified by a function of net solidity (*Sn*). Tsukrov et al. (2011) found through experiments that it is not sufficient to predict the drag coefficients of net panels only by *Sn*. By conducting experiments with a sphere, Lader et al. (2014) proposed that the geometry of the knot in a net structure have major impact on the drag force. Tang et al. (2018) found that the Reynold's number (*Re*), solidity ratio, attack angle, knot type and twine construction were all related to the hydrodynamic coefficient of netting panels. However, all of these parameters are difficult to implement in numerical models, and thus, secondary parameters are ignored in order to make the numerical solver feasible. However, none of these researchers have explicitly compared the performance of different fish cage shapes with varying dimensions, weights and current velocities.

The most widely used fish cage shapes in Norwegian waters are either circular or squared and are illustrated in Figure 3. Previously, squared fish cages were the main shape used in fish farms, while circular fish cages are currently trending. Since circular and squared fish cages are widely implemented in Norwegian fish farms, these cages are chosen for this study. Fish cages are gradually increased to produce more fish, and thus it is important to investigate whether fish cages should increase in the horizontal or vertical direction. Typical Norwegian sea-areas are not limited by the water depth, and thus not limited by the vertical distance of fish cages.

<div align="center">(a)   (b)</div>
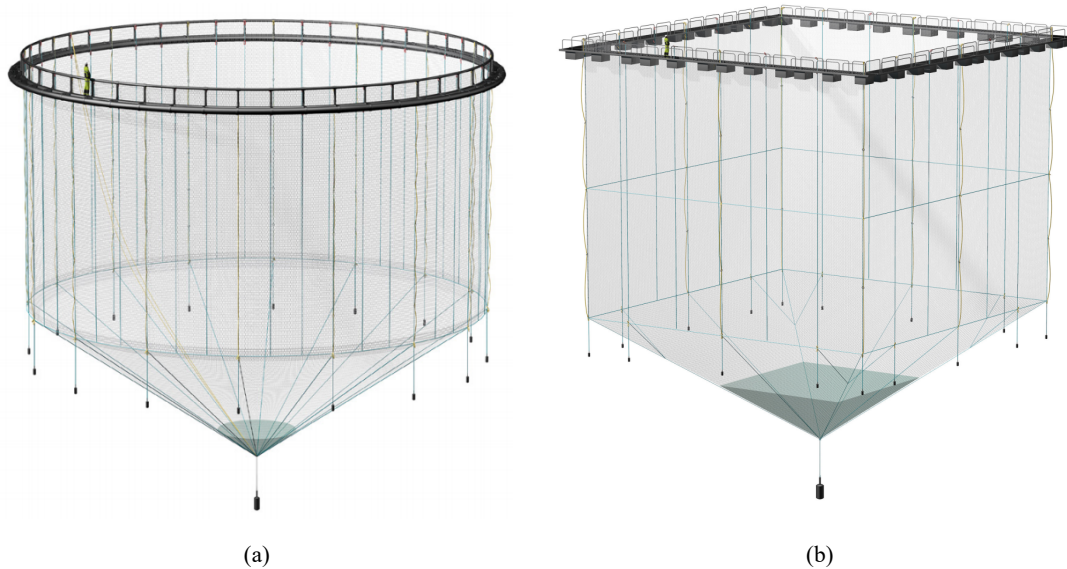
Figure 3. Illustration of the two fish cage shapes. (a) is a circular fish cage and (b) is a squared fish cage, where multiple sinker weights and a bottom centre weight are attached. The illustrations are gathered from a user manual, created by Egersund net (EgersundNet, 2020).

1.2. Scope and thesis outline

The purpose of the thesis is to carry out a comprehensive comparison between the circular and squared fish cage with different dimensions and weights, under pure current conditions. The structural solver and hydrodynamic models for the present structural analyses are given in Section 2. In Section 3, the two fish cage models are presented with the key parameters for measurement. Finally, the results are discussed in Section 4 with following concluding remarks in Section 5. The scope and outline of the thesis is presented in Figure 4.

1 Introduction
General descriptions of aquaculture, fish farm construction, environmental conditions and research are defined.

2 Numerical method
The structural model is presented with key equations which are invoked in the numerical solver. Hydrodynamic models are presented with supplementary theories and coefficients. The simulation process of the finite element solver, Code_Aster, is presented.

3 Description of the fish cage models
The two fish cage models are presented with respective dimensions and parameters. In addition, methods to calculate the cultivation volume, convergence study of the cross-section area and measurement of the fish cage height are given.

4 Results and discussion
The fish cages are discussed against the key parameters of measurement: drag force, cultivation volume, fish cage height and cross-section area.

5 Conclusions and future work
The predominant results are presented in the last section, with additional comments regarding future work.

Figure 4. Outline and scope of present thesis.

2. Numerical method

2.1. Structural model

2.1.1. Governing equations

In the present study, Code_Aster is used as the structural solver to calculate the structural responses of fish cages. The open source Code_Aster, is developed by EDF R&D (de France, 1989), and is well verified according to research done by Févotte and Lathuilière (2017), and offers 400 finite element typologies for the discretisation of solids. The broad range of solvers makes Code_Aster suitable for structural analysis of fish cages.

The fish cage netting can be divided into a set of elements, where the structural responses are calculated based on a FEM. By using the Cartesian coordinate system, the motions of Lagrangian nodes can be expressed with the same differential equations as Tsukrov et al. (2003):

$$[M]\ddot{q} + [K]q = F_g + F_b + F_h \tag{1}$$

where q is the time-dependent vector of nodal displacements, M is the mass matrix, K is the stiffness matrix, F_g is the nodal force vector due to gravity, F_b is the nodal force vector due to buoyancy, and F_h is the nodal force vector for the hydrodynamic forces. The environmental loads acting on submerged nettings are on the right side of Eq. (1). The nodal force vector F_h for a Screen model are calculated based on the following equation:

$$F_h = \frac{1}{2}C_d\rho_{fluid}A|u - v|(u - v) \tag{2}$$

where C_D is the coefficient of drag, A is the projected area of twines and u and v are the fluid and structure velocities. The remaining force vectors, F_g and F_b, are simply obtained and are only calculated at the initialisation step, which after, remain constant throughout the numerical

simulation process. The system is highly nonlinear because of the last term (F_h), on the right-hand side of Eq. (1), which is dependent on the time, the square of nodal velocities, and the structural deformations.

According to Antonutti et al. (2018), the system nonlinearity can cause high-frequency oscillations and bring challenges for the simulations to convergence. These oscillations commonly occur in structural mechanics and are solved by introducing damping. In the present structural solver, Eq. (1) is solved by utilizing the unconditionally stable Hilber-Hughes-Taylor-α (HHT-α) method, proposed by Hilber et al. (1977). With a continuous variable timestep, the HHT-α method introduces low numerical damping in the low-frequency band and high damping at the high-frequency band (Antonutti et al., 2018). By implementing the HHT-α in Eq. (1), the discretised form in time can be expressed as:

$$M\ddot{x}_{i+1} + (1 - \alpha)Kx_{i+1} + \alpha Kx_i = (1 - \alpha)\left(F_g + F_b + F_h\right)_{i+1} + \alpha\left(F_g + F_b + F_h\right)_i \quad (3)$$

where the relation for the HHT-α is obtained together with the displacements and velocities in the following equations:

$$x_{i+1} = x_i + \Delta t x_i + \Delta t^2[(0.5 - \beta)\ddot{x}_i + \beta\ddot{x}_{i+1}] \quad (4)$$

$$\dot{x}_{i+1} = \dot{x}_i + \Delta t[(1 - \gamma)\ddot{x}_i + \gamma\ddot{x}_{i+1}] \quad (5)$$

where the parameters α, β and γ are satisfied:

$$0 \le \alpha \le \frac{1}{3}, \qquad \beta = \frac{(1 - \alpha)^2}{4}, \qquad \gamma = \frac{1}{2} + \alpha \quad (6)$$

2.1.2. Finite element construction

The structural element used in the present study is a one-dimensional finite element denoted as "CABLE" in the structural solver, which was initially developed to calculate the mechanical behaviour of overhead electrical lines. This element is a version of the classic two-node "bar" element but can only bear tensions. It is suitable for representing highly flexible line-like structures (Antonutti et al., 2018), and thus, suitable for modelling of nettings. As illustrated in Figure 5, one "CABLE" element contains six nodal degrees of freedom (DOFs, three components at each node) in the global coordinate system, which correspond to the translations at its two nodes. Linear shape functions (N) are used to express the deformation of the element ($\hat{q}$) in the global coordinate system as a function of the vector of DOF (q):

$$\hat{q} = \begin{bmatrix} 1-\xi & 0 & 0 \\ 0 & 1-\xi & 0 \\ 0 & 0 & 1-\xi \end{bmatrix} \begin{bmatrix} q_x^i \\ q_y^i \\ q_z^i \end{bmatrix} + \begin{bmatrix} \xi & 0 & 0 \\ 0 & \xi & 0 \\ 0 & 0 & \xi \end{bmatrix} \begin{bmatrix} q_x^j \\ q_y^j \\ q_z^j \end{bmatrix} \tag{7}$$

where ξ is the strain, and the two square matrixes are the shape functions (N).
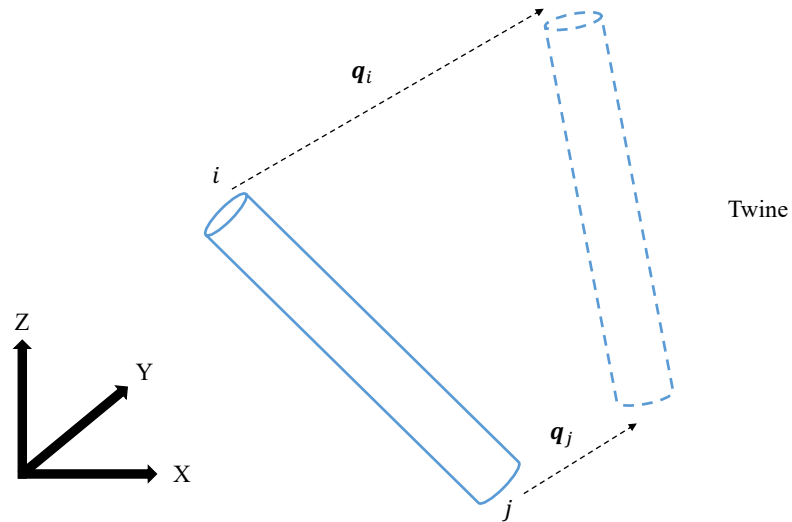
Figure 5. Illustration of the "CABLE" element with six nodal degrees of freedom.

The mass matrix (M) and stiffness matrix (K) from Eq. (1) for a single structural element are given as:

$$[M] = \frac{\rho_s \pi d_{ws}^2}{4} \int_{x=0}^{L} NN^T \, dx \qquad (8)$$

$$[K] = \frac{\pi d_{we}^2 E}{4} \int_{x=0}^{L} BB^T \, dx \qquad (9)$$

where $B = J^{-1} \frac{\partial N}{\partial x}$ is the element strain-displacement transformation matrix, J is the Jacobian matrix, d_{ws} is the structural diameter, d_{we} is the elastic diameter, and L is the length of one element. After assembling contributions from individual elements and concentrating all the environmental loads to nodes, the structural responses can be calculated using Eq. (1). In practice, a mesh grouping method is usually adopted in the modelling to reduce the computational effort. In order to achieve equivalent numerical results, the derived diameters d_{ws} and d_{we} are applied during the construction of the model. The detailed derivation and explanation of the derived diameters can be referred to Cheng *et al.* (2020). Here, only the relationships between the derived diameters and the physical twine diameter (d_{w0}) for nettings with square meshes are presented:

$$d_{ws} \approx \sqrt{\lambda} d_{w0}; \quad d_{we} = \sqrt{\lambda} d_{w0}; \qquad (10)$$

where λ is mesh grouping factor which is defined as the ratio between the mesh size of the numerical netting and the physical netting.

While nodes are subjected to displacement, the floating collar, which can be considered a curved beam, is subjected to loads caused by elastic deformations (Strand and Faltinsen, 2020). The floating collar can be divided into multiple curved beam elements, with a constant section (accounting transverse shearing) and a constant radius of curvature. The beam elements in Code_Aster are described in the documentation made by PROIX et al. (2019).

In practice, the floating collar contributes to structural responses, but this contribution is not deployed in this study. The structural responses are purely based on the nettings, ropes and auxiliary weights attached to the fish cages, which have larger contributions than the floating collar. The circular floating collar, which is constructed with HDPE pipes, is limited by the torsion in the pipes (Cardia and Lovatelli, 2015). The floating collar is also selected to provide an adequate buoyancy force for the exposed site.

2.2. Hydrodynamic model

2.2.1. Hydrodynamic model for netting

Several researchers (Balash et al., 2009, Tsukrov et al., 2011, Lader et al., 2014, Tang et al., 2018) have found, through experiments, that the hydrodynamic characteristics are mainly dependent on two dimensionless variables, Re and Sn. By definition, Sn is the percentage of structural blockage of a flow (Klebert et al., 2013), and can be expressed as:

$$Sn = \frac{2d_w}{L} - \left(\frac{d_w}{L}\right)^2 \tag{11}$$

where d_w is the twine diameter and L is the half mesh size, illustrated in Figure 6. The solidity ratio for realistic fish farms are within 0.19-0.43, including biofouling (Kristiansen and Faltinsen, 2012). In the present study, an ideal knotless mesh is implemented in the numerical model.

The second dimensionless variable is Re, which is defined as:

$$Re = \frac{U d_w}{\nu} \tag{12}$$

where U is the undisturbed fluid velocity, d_w is the twine diameter and ν is the kinematic viscosity of the fluid. The typical Reynold's number for fish cage nettings lies in the range of 100-10000 (Cheng et al., 2020a).
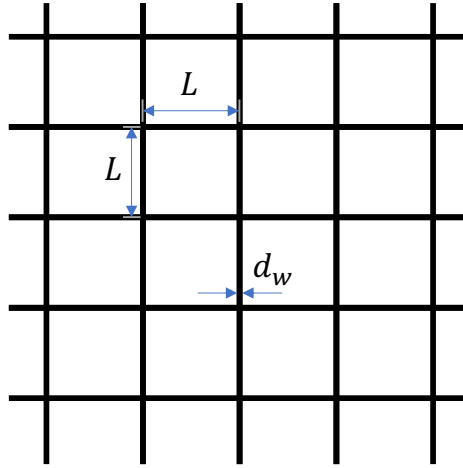
Figure 6. Illustration of the twine diameter d_w and half mesh size L for a square-mesh netting.

As the hydrodynamic forces on netting are complex, a hydrodynamic force model is required to calculate the forces on structures and transfer the forces to the structural solver. Several studies (Patursson et al., 2010, Bi et al., 2014, Chen and Christensen, 2016) have calculated the hydrodynamic forces with the usage of Morison model.

In the present study, hydrodynamic forces on nettings are calculated based on Screen models, which are theoretically superior to Morison models, as the twine-to-twine interaction is implicitly included in the force calculation (Cheng et al., 2020a). Figure 7 illustrates a screen model that is used in the present study to calculate the hydrodynamic forces (F_h) on the netting. The hydrodynamic forces are decomposed into drag force F_D Eq. (13) and lift force F_L Eq. (14):

$$F_D = \frac{1}{2} C_D \rho_w A_t |U_c - v|^2 i_D \tag{13}$$

$$F_L = \frac{1}{2} C_L \rho_w A_t |U_c - v|^2 i_L \tag{14}$$

where ρ_w is the fluid density, A_t is the area of the net panel, U_c is the velocity of the fluid at the centroid of the net panel and v is the velocity of the structure. The unit vectors $\boldsymbol{i_D}$ and $\boldsymbol{i_L}$ which are used to indicate the directions of drag and lift force and are defined by Eqs. (15) and (16). C_D and C_L are the drag and lift force coefficients in the Screen model, respectively.
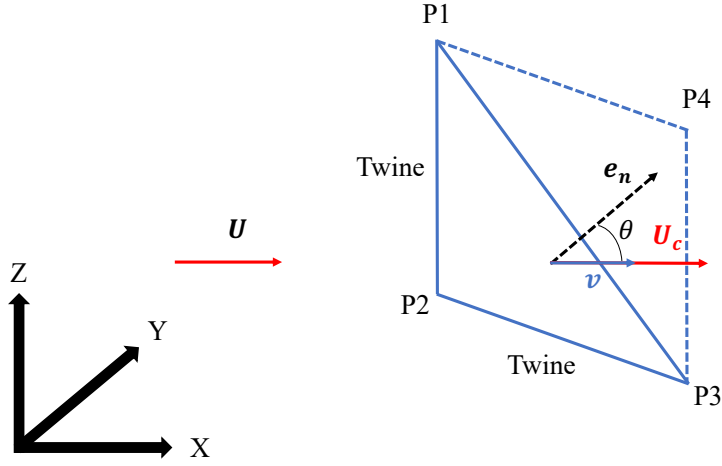
Figure 7. Illustration of a Screen model. The inflow angle θ of the net-panel element is the angle between $\boldsymbol{e_n}$ and $\boldsymbol{U_c}$.

The unit force vectors $\boldsymbol{i_D}$ and $\boldsymbol{i_L}$, which are used to indicate the directions of drag and lift forces, are calculated with the following equations:

$$\boldsymbol{i_D} = \frac{\boldsymbol{U_c} - \boldsymbol{v}}{|\boldsymbol{U_c} - \boldsymbol{v}|} \tag{15}$$

$$\boldsymbol{i_L} = \frac{(\boldsymbol{U_c} - \boldsymbol{v}) \times \boldsymbol{e_n} \times (\boldsymbol{U_c} - \boldsymbol{v})}{|(\boldsymbol{U_c} - \boldsymbol{v}) \times \boldsymbol{e_n} \times (\boldsymbol{U_c} - \boldsymbol{v})|} \tag{16}$$

where the unit normal vector of the net panel $\boldsymbol{e_n}$ is expressed as:

$$\boldsymbol{e_n} = \frac{\overrightarrow{P1P2} \times \overrightarrow{P1P3}}{\left|\overrightarrow{P1P2} \times \overrightarrow{P1P3}\right|} \tag{17}$$

The force coefficients employed in this study are originally proposed by Kristiansen and Faltinsen (2012), and are expressed as Eqs. (19)-(26). The drag and lift coefficients are expressed respectively as:

$$C_D = C_{D0}(0.9cos\theta + 0.1cos3\theta) \tag{19}$$

$$C_L = C_{L0}(sin2\theta + 0.1sin4\theta) \tag{20}$$

$$C_{D0} = C_{cylinder}\frac{Sn(2 - Sn)}{2(1 - Sn)^2} \tag{21}$$

$$C_{L0} = \frac{0.5C_{D0} - C_{L45}}{\sqrt{2}} \tag{22}$$

$$C_{L45} = \frac{\pi C_{N45}}{8 + C_{N45}} \tag{23}$$

$$C_{N45} = C_{cylinder}\frac{Sn}{2(1 - Sn)^2} \tag{24}$$

$$
\begin{aligned}
C_{cylinder} = &-78.46675 + 254.73873(log_{10} Re) - 327.8864(log_{10} Re)^2 \\
&+ 223.64577(log_{10} Re)^3 - 87.92234(log_{10} Re)^4 + 20.00769(log_{10} Re)^5 \\
&- 2.44894(log_{10} Re)^6 + 0.12479(log_{10} Re)^7
\end{aligned} \tag{25}
$$

$$Re = \frac{d_{w0}(\boldsymbol{U_c} - \boldsymbol{v})}{v(1 - Sn)}, \qquad 10^{3/2} \leq Re \leq 10^4 \tag{26}$$

2.2.2. Hydrodynamic model for floating collar and cables

For the anchor lines and the HDPE floating collar, the hydrodynamic forces are calculated based on the Morison model introduced by Morison et al. (1950). The hydrodynamic forces are decomposed into the two components, *i.e.*, normal drag force ($\boldsymbol{F_n}$, Eq. (27)) and tangential drag force ($\boldsymbol{F_t}$, Eq. (28)), which are expressed as:

$$\boldsymbol{F_n} = \frac{1}{2} C_n \rho L d_w |\boldsymbol{u^r}_n| \boldsymbol{u^r}_n \tag{27}$$

$$\boldsymbol{F_t} = \frac{1}{2} C_t \rho L d_w |\boldsymbol{u^r}_t| \boldsymbol{u^r}_t \tag{28}$$

where L is the length of anchor lines or HDPE pipes, d_w is the section diameter, ρ is the fluid density. $\boldsymbol{u^r}_n$ and $\boldsymbol{u^r}_t$ are the normal and tangential velocity of fluid relative to the twine. C_n and C_t are the normal and tangential drag coefficients. The two force coefficients employed in this study originates from DeCew et al. (2010), and are expressed by Eqs. (29) - (32). A 2D illustration of the force decomposition is given in Figure 8.

$$C_n = \begin{cases} \frac{8\pi}{sRe}(1 - 0.87s^{-2}) & 0 < Re < 1 \\ 1.45 + 8.55Re^{-0.9} & 1 < Re < 30 \\ 1.1 + 4Re^{-0.5} & 30 < Re < 2.33 \times 10^5 \\ -3.41 \times 10^{-6}(Re - 5.78 \times 10^5) & 2.33 \times 10^5 < Re < 4.92 \times 10^5 \\ 0.401\left(1 - e^{-\frac{Re}{5.99} \times 10^5}\right) & 4.92 \times 10^5 < Re < 10^7 \end{cases} \tag{29}$$

$$C_t = \pi\mu\left(0.55\sqrt{Re} + 0.084Re^{\frac{2}{3}}\right) \tag{30}$$

$$s = -0.077215665 + ln(8/Re); \tag{31}$$

$$Re = \frac{\rho d_w(u_n - v_n)}{\mu} \tag{32}$$
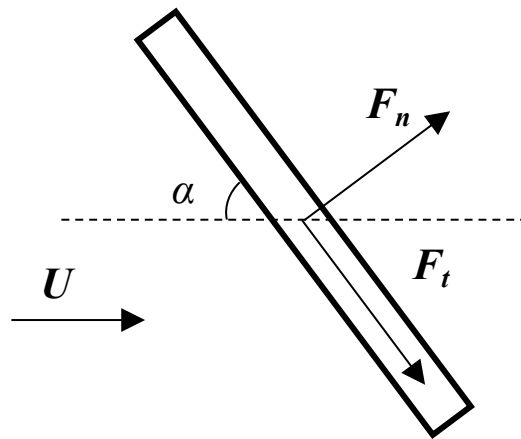
Figure 8. A 2D illustration of the hydrodynamic forces on cables or pipes. F_n and F_t are the normal and tangential drag forces, respectively. The angle of attack α is the angle between the current direction and the axis of the cable or pipes.

2.3. Simulation process

In the present study, 1200 simulations of numerical fish cages are deployed to compare the two fish cage models for different dimensions, weights and current velocities. In order to present adequate results of the structural responses, the fish cages are exposed to a pure current velocity for 60 s, with a time step of 0.1 s, where the mean value of the last 10 seconds is used to compare the results. At the start of the simulation process, the fish cages are affected by the sinker weights which causes strong initial drag forces and damping of the weights. This is illustrated in Figure 9, where the fish cage reaches a stable state after roughly 30 s. Large current velocities causes oscillating drag forces, due to large structural responses from the velocity.

Time history drag force
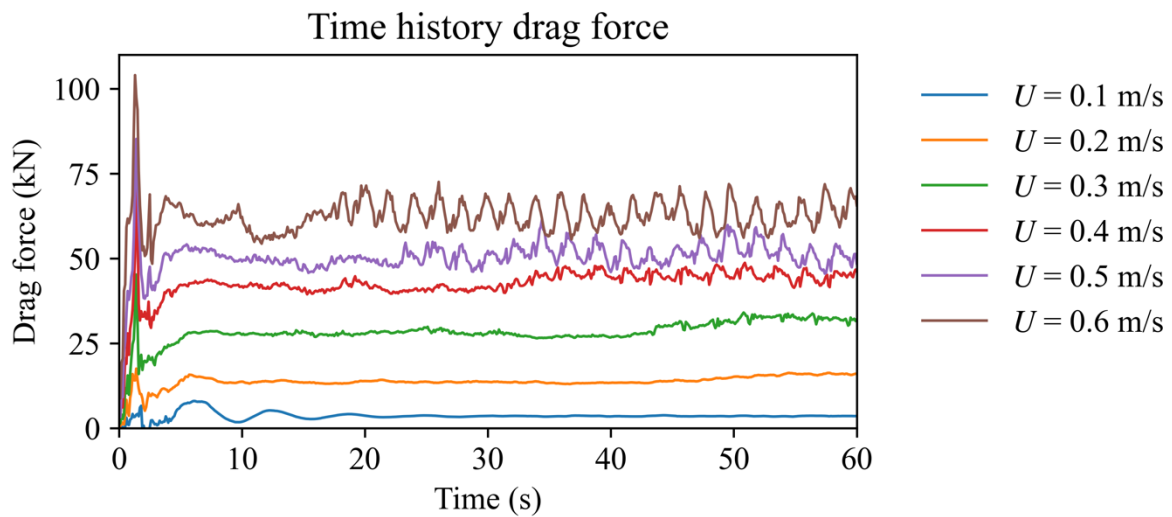
Figure 9. Time history of the drag force on the fish cages for the full duration time-series. The fish cage refers to the circular cage, where $C = 150$ m, $H = 20$ m and $W = 60$ kg/m.

An illustration of the numerical simulation process is presented in Figure 10, where an external module is invoked at each time step to calculate the hydrodynamic forces on the nets, cables and HDPE pipes and maps the forces onto corresponding nodes in the structural elements. Two types of hydrodynamic models, *i.e.* Screen model and Morison model, are applied to nettings and cables, respectively.
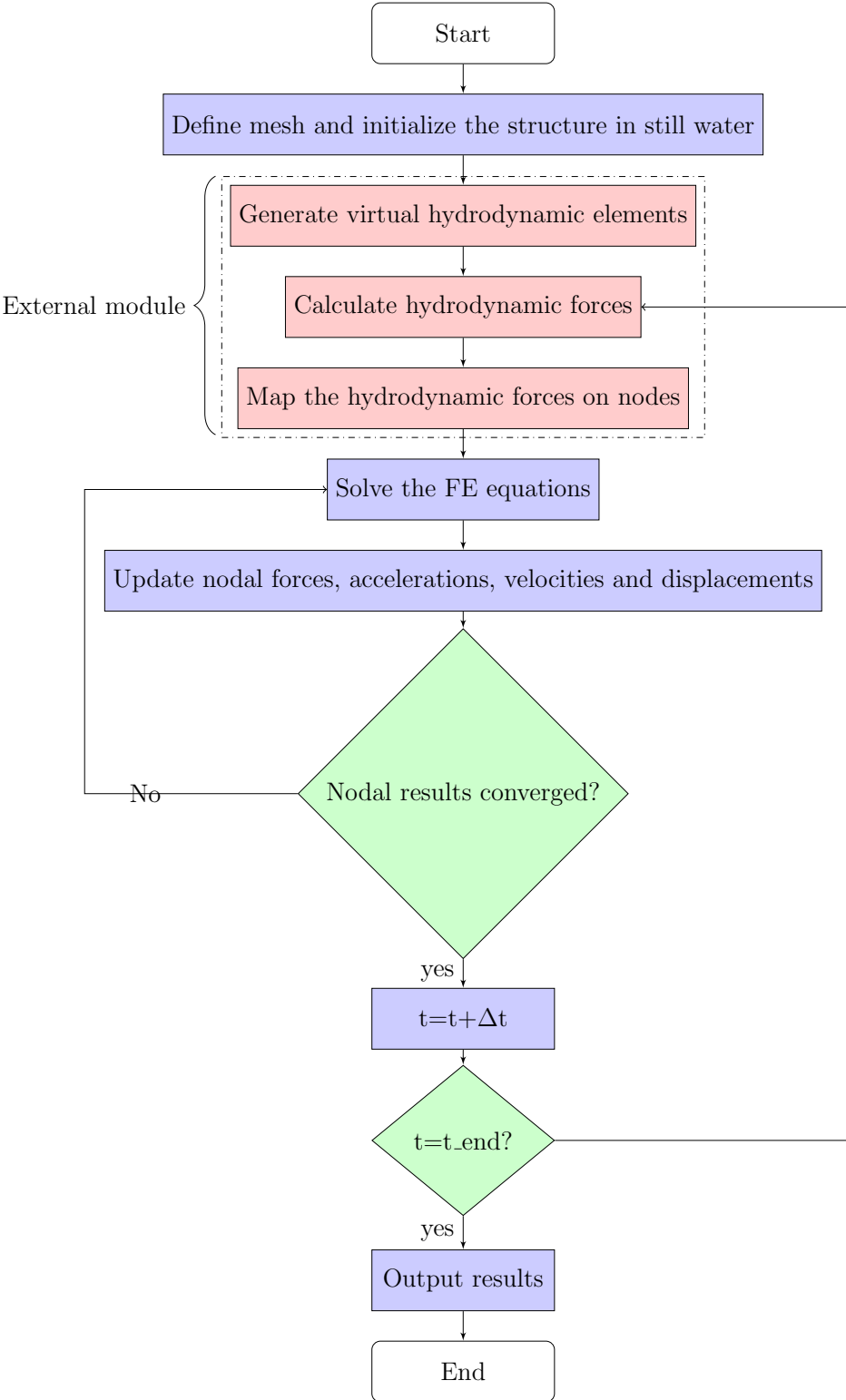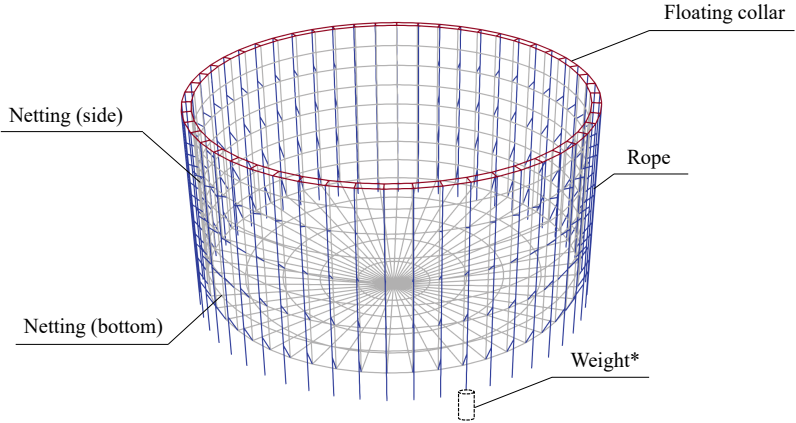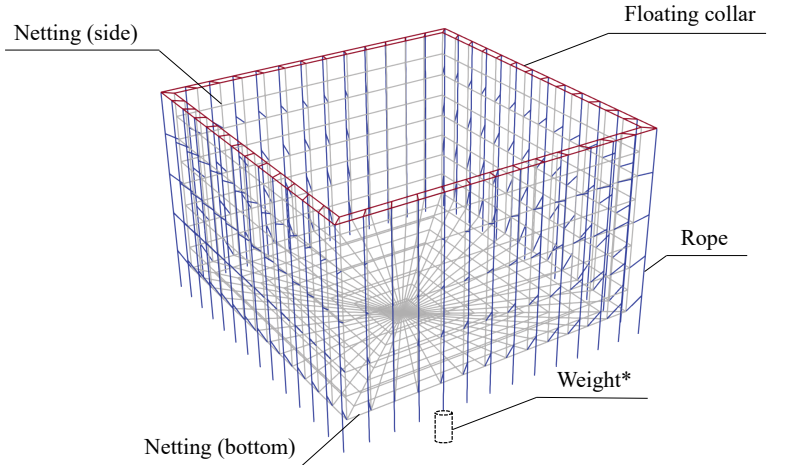
Figure 10. Reproduction of the simulation process for the numerical solver originally proposed by Cheng et al. (2020a).

3. Description of the fish cage models

3.1. Fish cage models in the present study

In the present study, two typical Norwegian fish cages are numerically modelled and compared under pure current conditions. The two cages are reproductions of fish cages provided by Egersund Net (part of AKVA Group ASA): one is a circular cage, the other is a squared cage. Both fish cage models have the same weight system with bottom sinker weights, as presented in Table 1. The coloured components refer to the floating collar (red), ropes (blue) and nettings (grey).

Table 1. Descriptions of the cage shapes and weight systems for the fish cages.

Fish cage	Cage shape
Circular	

| Squared | |

*Note: Although the illustrations only plot one weight, multiple weights are assembled at the lower end of the ropes.

The nettings in the two fish cages have the same following parameters: solidity (Sn) of 0.25, twine diameter (d_w) of 1.5 mm and a half mesh length (L) of 12 mm. The material properties of the nettings are assigned with a Young's modulus (E) of 200 MPa and a density of 1120 kg/m^3 to represent the Nylon material. The solidity in the present study indicates a realistic fish cage with little biofouling as aforementioned in Section 1. For all cases, the netting has a cone shape at the bottom with a cone height of 3 m.

The ropes attached to the floating collar have a section diameter of 50 mm and are 1 m longer than the cage design height. The material of the rope is Polyethylene (PE) with Young's modulus (E) of 300 MPa and density of 1100 kg/m^3. The weights are attached to the lowest end of the ropes.

The dimensions of the two fish cages, weights and current velocities used in the present study are given in Table 2. The dimensions of the fish cage include circumference (C) and design height (H). The weight (W) is measured per meter according to the report by Cardia and Lovatelli (2015). The current velocity (U) is assumed uniform within the water depth.

Table 2. Specification of the dimensions of cage, weights and current velocities for the simulations.

Parameter	Variable	Value	Unit
Circumference	C	120, 130, 150, 160, 180	m
Design height	H	10, 20, 30, 40, 50	m
Weight*	W	40, 50, 60, 70	kg/m
Current velocity	U	0.1, 0.2, 0.3, 0.4, 0.5, 0.6	m/s

*Note: In the present study, the weight refers to the submerged weight per meter of circumference (Cardia and Lovatelli, 2015). E.g., for a weight of 40 kg/m, the total weight on a fish cage with 120 m circumference is 40×120 = 4 800 kg.

3.2. Key parameters for measurement

3.2.1. Fish cage volume

Currently, there are several methods to calculate the volume of fish cages. Previously, a number of researchers (DeCew et al., 2013, Qu et al., 2019, Cheng et al., 2020b, Chen et al., 2021) estimated fish cage volumes with numerical approaches. In this study, the fish cage volume is calculated with two different methods, *i.e.,* the scalar triple product method and the divergence method. Typically, the scalar triple product method is the predominant method used to calculate

Numerical study of two typical Norwegian gravity-based fish cages with different cage shapes and weights

the fish cage volume of numerical fish cages and is illustrated in Figure 11. This method was initially proposed by Huang et al. (2006), in order to estimate a volume reduction coefficient. The divergence method is illustrated in Figure 12 and is implemented in this study to compare the two volume methods.
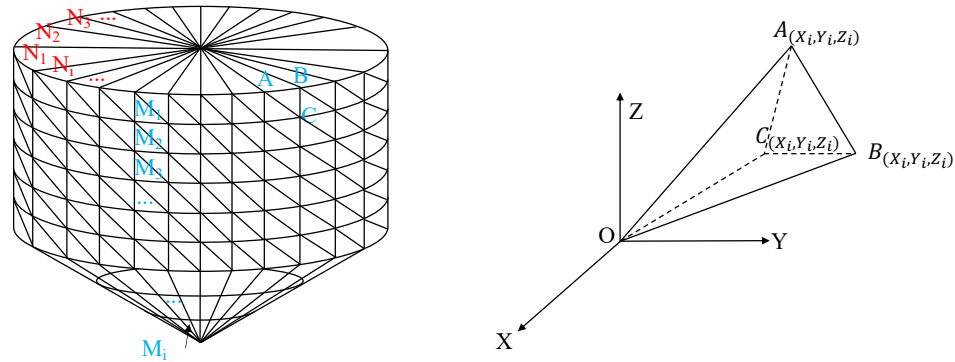
Figure 11. Illustration of the scalar triple product method. The left figure represents the volume of a fish cage in its initial undeformed state. Reproduction from work done by Xu and Qin (2020).

From the central origin of the cage in Figure 11, tetrahedron elements are constructed within each level "M". With these tetrahedrons, the scalar triple product method can be utilized in order to calculate the fish cage volume:

$$\forall = \sum_{i=1}^{N} \frac{1}{6} |A \cdot (B \times C)| \tag{33}$$

where the volume is represented as $\forall$, N is the number of tetrahedron elements to embrace the volume and A, B and C are the coordinates of the vertices in each tetrahedron.
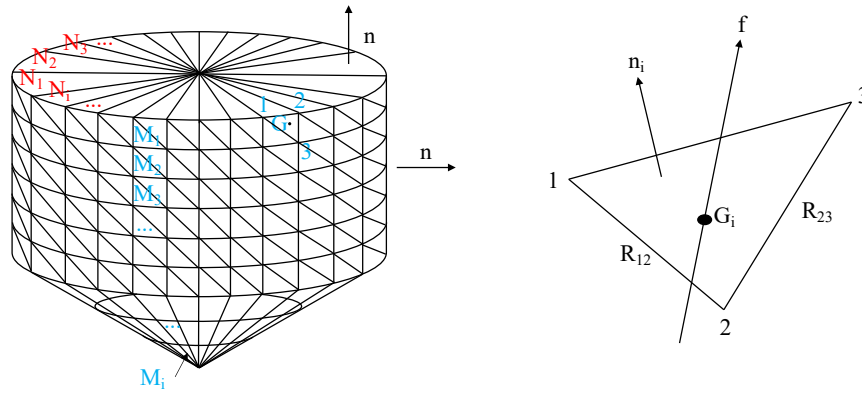
Figure 12. Illustration of the divergence method. The left figure represents the volume of a fish cage in its initial undeformed state. Reproduction from work done by Xu and Qin (2020).

The divergence method is a vector operator, which utilizes Gauss's theorem:

$$\iiint_\Delta (\nabla \cdot f) d\forall = \oiint_S (f \cdot n) dA_s \qquad (34)$$

where f is a continuous differentiable vector, n is the respectably normal vector of the surface plane and A_s is the surface area of the surrounded volume. If the left-hand side of the equation represents the entire volume, the term $\nabla \cdot f = 1$ becomes the total volume of the enclosed surface S (Xu and Qin, 2020). By implementing the divergence theorem to each element and summate all triangles shown in Figure 12, the volume of the fish cage can be expressed with the following equation:

$$\forall = \sum_{i=1}^{N} \left(x_{G_i} i + y_{G_i} j + z_{G_i} k \right) \cdot \frac{R_{12i} \times R_{23i}}{|R_{12i} \times R_{23i}|} \Delta A_i \qquad (35)$$

where G_i is the geometric centre of the triangle, R_{12i} and R_{23i} are the normal unit vectors from the triangular points [p1, p2, p3] and ΔA_i is the area of each triangle.

3.2.2. Volume factor

In addition to calculating the total cultivation volume of the fish cage, the cage deformation is measured against the initial fish cage volume and is expressed as a volume factor. The volume factor is defined as a fraction between the volume when the fish cage is subjected to the velocity and the initial fish cage volume, and it is expressed as:

$$\frac{V}{V_0} \tag{36}$$

where V is the mean volume of the last 10 seconds of the simulation process and V_0 is the initial volume in still water.

At the initial time step of the numerical simulation process, the volume of the fish cage is not affected by the auxiliary weights. When the simulation initiates, the current velocity and weights influence the netting. This influence causes a stretch of the nettings in the vertical direction, which increases the total cultivation volume. Thus, the volume factor may be more than one for small current velocities where the cage deformation is limited.

As shown in Figure 13, the two methods for estimating the cultivation volume have similar results. The largest deficit between the two methods is less than 3.5 %, indicating that the methods have the same level of accuracy for the volume estimation. In order to compare the computational efficiency of the two volume estimation methods, a trial case is carried out using the squared fish cage with $C = 120$ m, $H = 10$ m, $W = 40$ kg/m and $U = 0.1$ m/s. In this trial case, the time-series of nodes' positions are read and passed to the two methods to calculate the cage volume. As the time-series results contain 600 time slices for the 60 s simulation, the functions to calculate the cage volume will be invoked 600 times. The total elapsed time is 16.3 s for the scalar triple product method, and 48.7 s for the divergence method. As the divergence method is almost 3 times slower than the scalar triple product method, the scalar triple product method is preferred and applied in the subsequent results and discussion section.
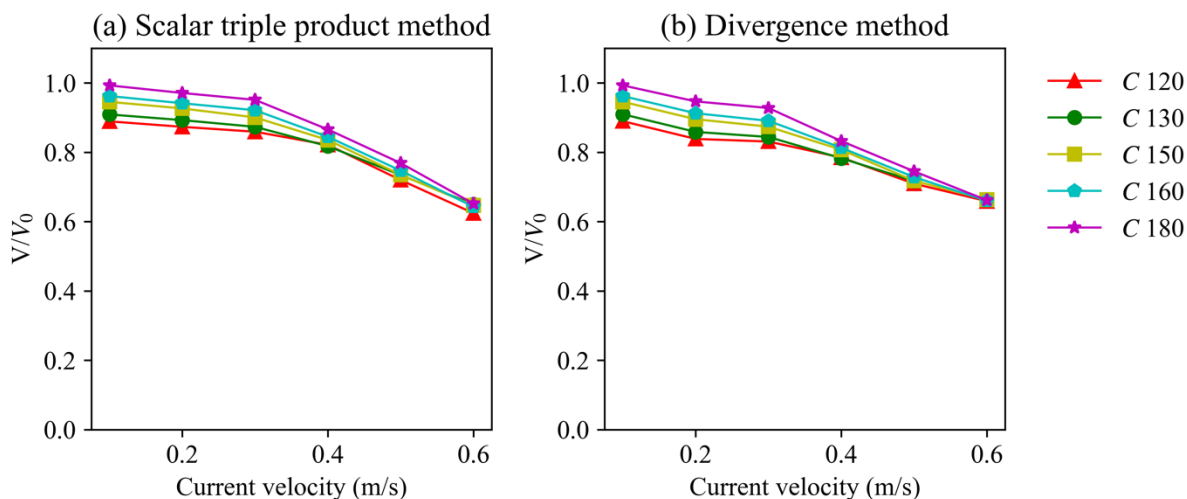
Figure 13. Comparison of the volume factor with the scalar triple product method and the divergence method. Both subfigures refer to the squared fish cage, where $H = 20$ m and $W = 50$ kg/m.

3.2.3. Cross-section area

The cross-section area is extracted by implementing a series of bounding boxes which surrounds the fish cage. By choosing an arbitrary point (0) as the default origin (in practice point $(0, 0)$), and defining n vectors from the origin, the cross-section area can be computed by using the principle of vector cross product of the outer limits of the area enclosed by the bounding boxes. Both the cross-section areas of the X-O-Z plane, illustrated in Figure 14 and the Y-O-Z plane, illustrated in Figure 15, are measured. In order to adequately calculate the cross-section area, a convergence study is performed to get a sufficient number of rectangles to calculate the cross-section area. Figure 16 shows the cross-section area for different numbers of bounding boxes, where an increased number of bounding boxes gradually converges towards the same cross-section area. When the number of rectangles is ≥ 6, the deviations between the areas are less than 1 %, indicating that 6 bounding boxes is adequate. For the discussion in Section 4.4, the X-O-Z plane is chosen as the reference plane for comparison of the cross-section areas of the two fish cages.
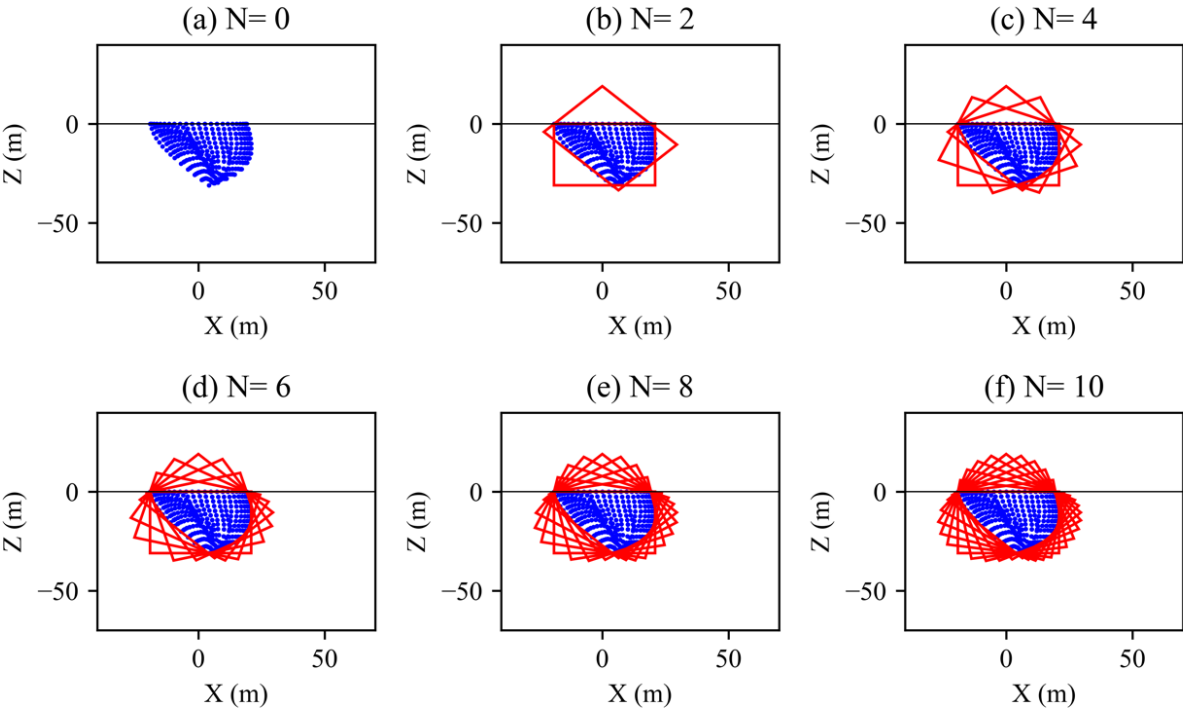
Figure 14. Illustration of bounding boxes surrounding the fish cage in order to extract the cross-section area in the X-O-Z plane. Each figure contains different number of bounding boxes (rectangles), ranging from 0 to 10, with an increase of two, for (a) to (f), respectively. All the fish cages refer to the circular fish cage, where $H = 20$ m.
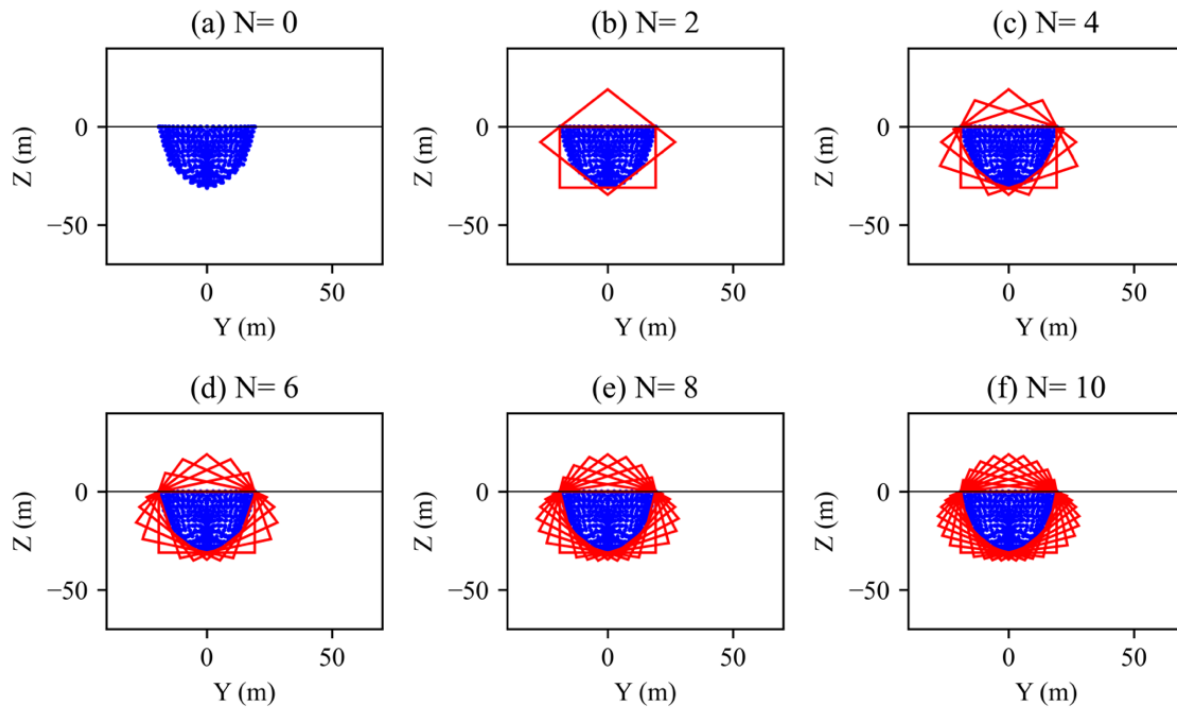
Figure 15. Illustration of bounding boxes surrounding the fish cage in order to extract the cross-section area in the Y-O-Z plane. Each figure contains different number of bounding boxes (rectangles), ranging from 0 to 10, with an increase of two, for (a) to (f), respectively. All the fish cages refer to the circular fish cage, where $H = 20$ m.
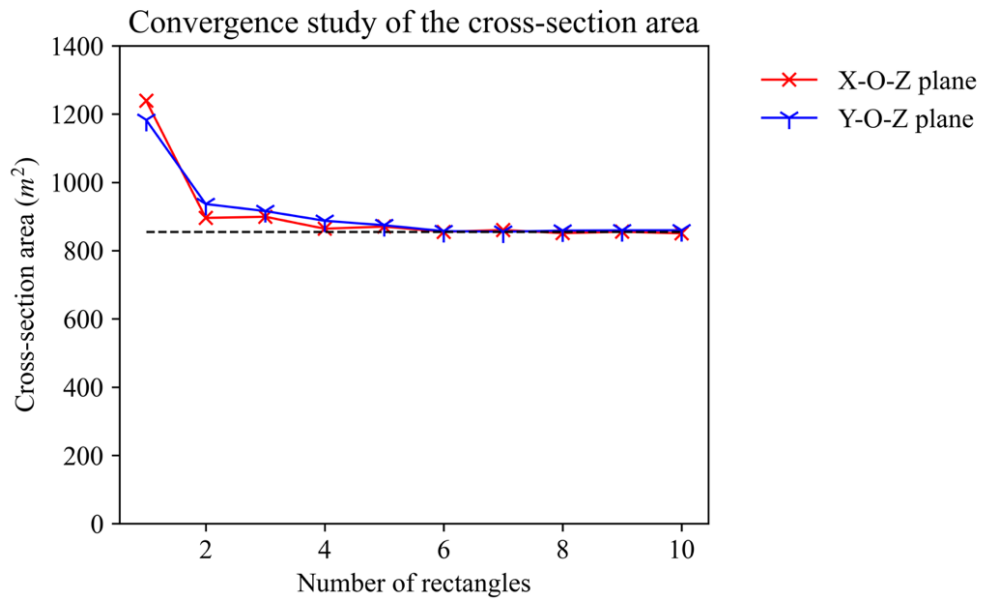
Figure 16. Convergence study of the cross-section with an increasing number of rectangles.

3.2.4. Fish cage height

In addition to the volume and cross-section area of the fish cage, the fish cage height is compared and is measured as the distance that joins the highest node with the lowest node of the fish cage nettings, as illustrated in Figure 17. As aforementioned in Section 3.2.2, the weight does not initially affect the fish cages in the simulation process, which results in a significant increase of the fish cage height during the simulation time-series.
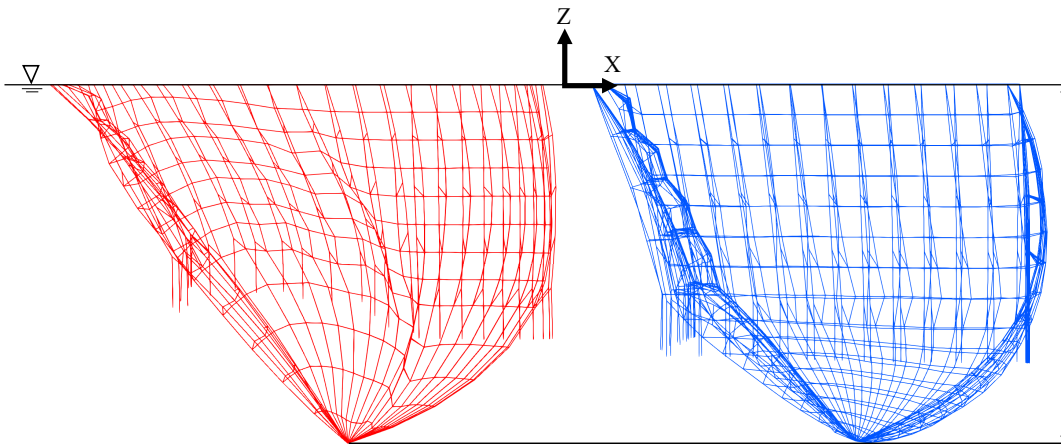
Figure 17. The fish cage height is measured as the distance from top of the main net to the lowest point of the bottom net. The red and blue cages represent the circular and squared cage, respectively.

4. Results and discussion

The following subsections evaluates the drag force, cultivation volume, volume factor, fish cage height and cross-section area with respect to different current velocities, cage dimensions (circumferences and design heights) and cage weights. Figure 18, 19 and 20 shows the deformation of the two fish cage models for different current velocities sectioned from the top, side and behind, respectively.

When the fish cages are exposed to strong current velocities, the squared cage sustains its initial cage shape more than the circular cage, given the same dimensions and weight. As the current velocity increases, the circular fish cage elongates in the current direction longer than the squared cage. Additionally, the nettings of the circular cage narrows towards the centre of the cage, as seen in Figure 20. The characteristic cage deformations and elongations, which derives from the shapes of the fish cages, are distinctive contributors which influences the comparison of the key parameters for measurements.
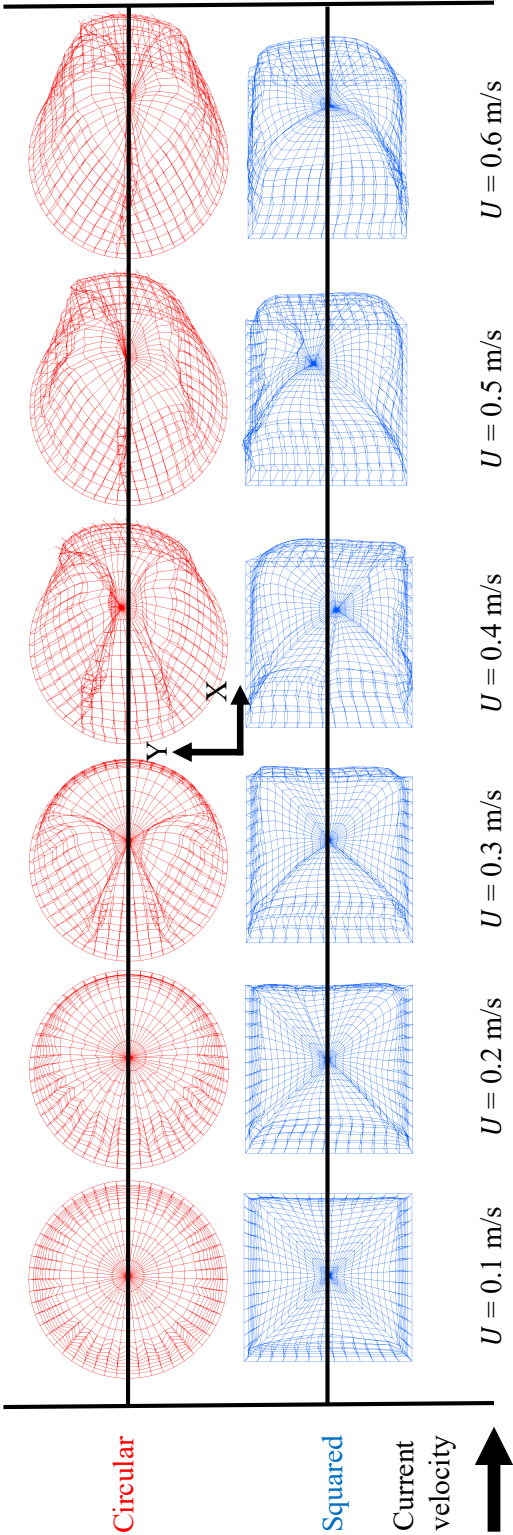
Figure 18. Assembly of the fish cage deformations with respect to varying current velocities where the circular (red) and squared (blue) cages are shown from the top. Both fish cage models have $C = 130$ m, $H = 20$ m and $W = 70$ kg/m.
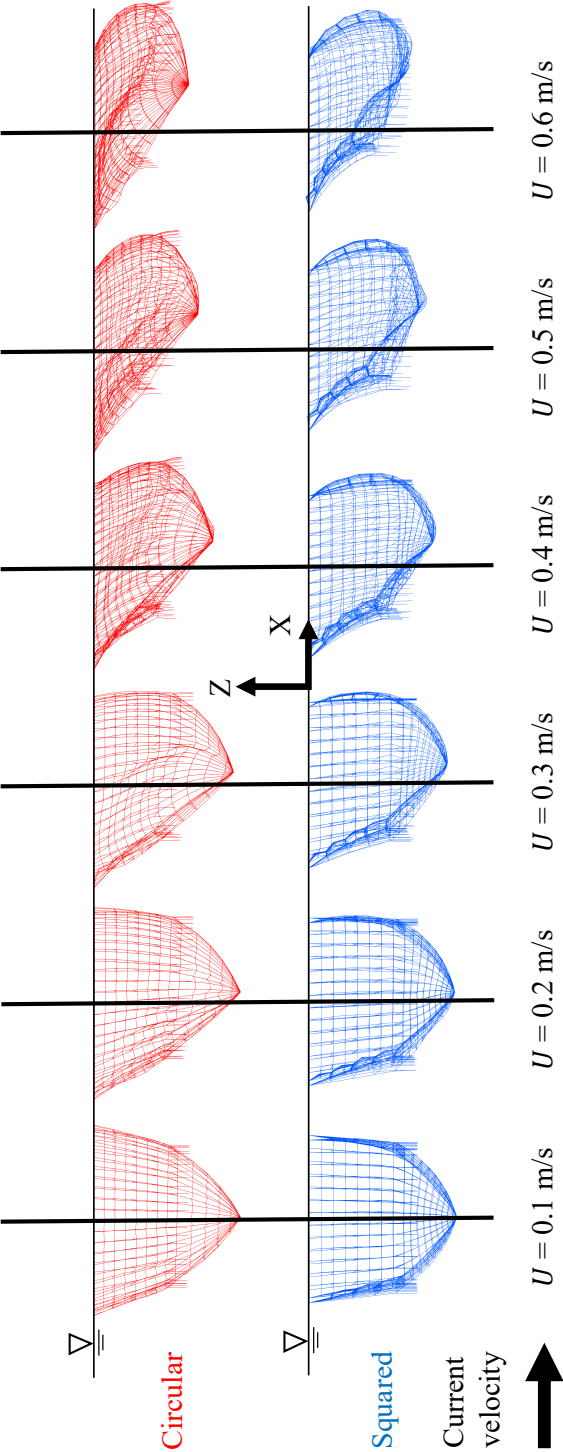
Figure 19. Assembly of the fish cage deformations with respect to varying current velocities where the circular (red) and squared (blue) cages are shown from the side. Both fish cage models have $C = 130$ m, $H = 20$ m and $W = 70$ kg/m.
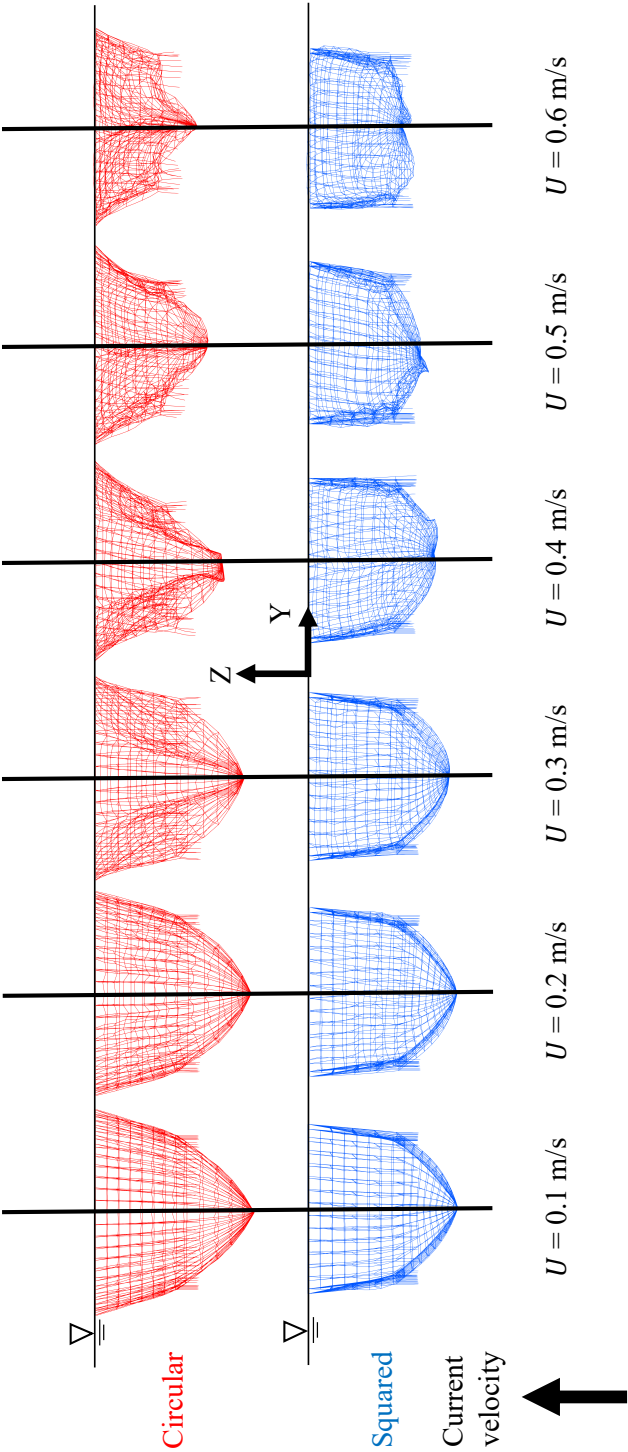
Figure 20. Assembly of the fish cage deformations with respect to varying current velocities where the circular (red) and squared (blue) cages are shown from behind. Both fish cage models have $C = 130$ m, $H = 20$ m and $W = 70$ kg/m.

4.1. Drag force

4.1.1. Drag forces under different current velocities

This section explicitly compares the drag force on the fish cages for different current velocities. Figure 21 shows the drag force on the two fish cages for different current velocities with varying design heights (horizontal) and circumferences (vertical). In general, the drag force exerted on the fish cages substantially increases with the velocity. Additionally, when the fish cages have the same dimensions and weight, the deficit between the drag force of the two cages increases in compliance with larger velocities.

The drag force exerted on the squared cage is greater than for the circular cage, for all respective cases, given that the fish cages have the same dimensions, weight and are subjected to the same velocity. The perceptive difference of the drag force between the two fish cages is a consequence of their distinct cage shapes, which is illustrated in Figure 22. Comparatively, the nettings for the circular cage are additionally stretched more than the squared cage, resulting in a more spacious section for the velocity to flow through. In addition, the nettings of the squared cage are compressed greater than the circular cage, which causes a congestion of nettings on the squared cage compared to the circular cage, as seen in Figure 22. The occurring congestion of the fish cage nettings for the squared fish cage, obstructs the incoming current velocity greater than the circular fish cage, which results in a larger drag force exerted on the squared cage than the circular cage.

As aforementioned at the start of Section 4, the squared cage sustains its initial cage shape greater than the circular cage, given the same dimensions and weight, when the fish cages are exposed to strong current velocities. The bottom nettings of both fish cages tend to drift such that the downstream end displace obliquely upwards in compliance with the current velocity. However, the upwards movement of the bottom nettings is only noticeable for current velocities larger than 0.2 m/s, as seen in Figure 19.
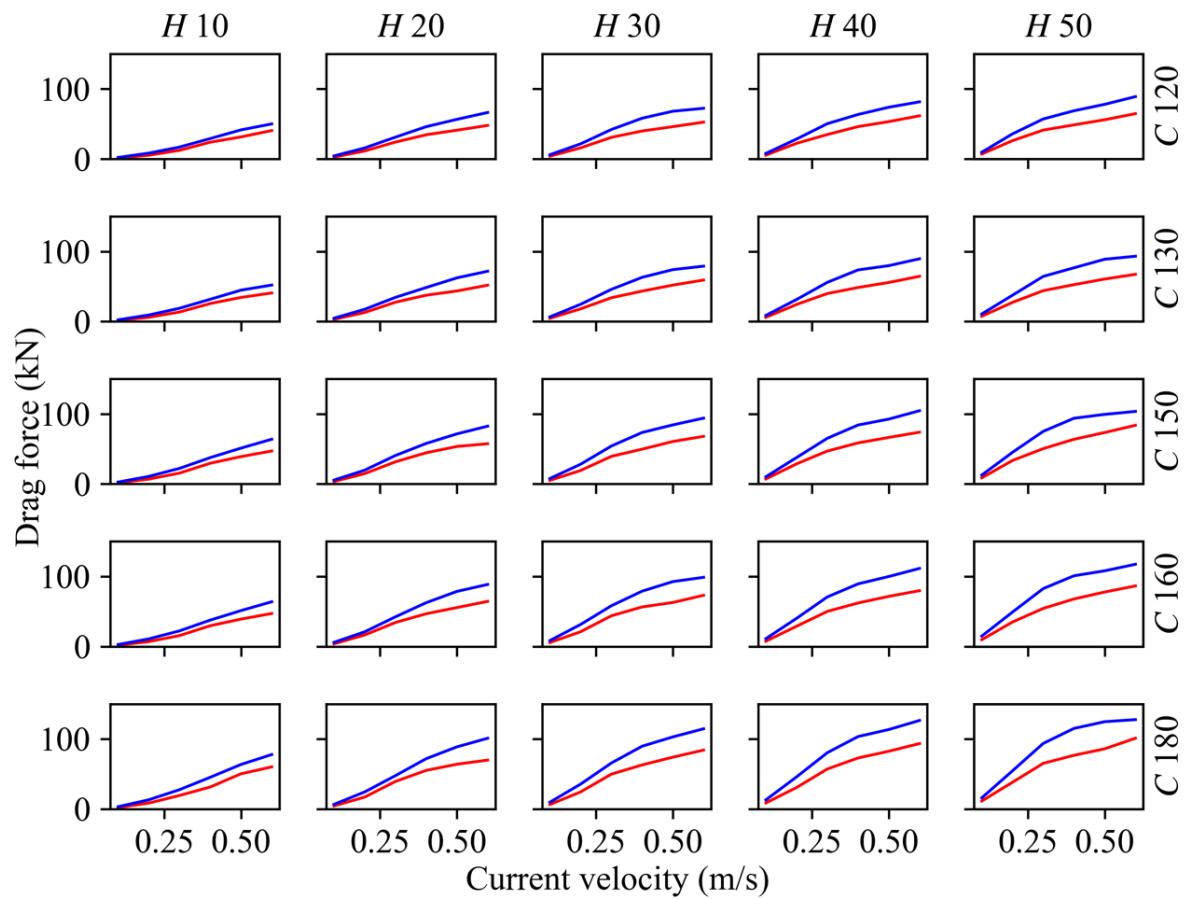
Figure 21. Illustration of the drag force on the two fish cages with the same $W = 50$ kg/m, but with different current velocities design heights and circumferences. The red and blue lines refer to circular and squared cage, respectively.
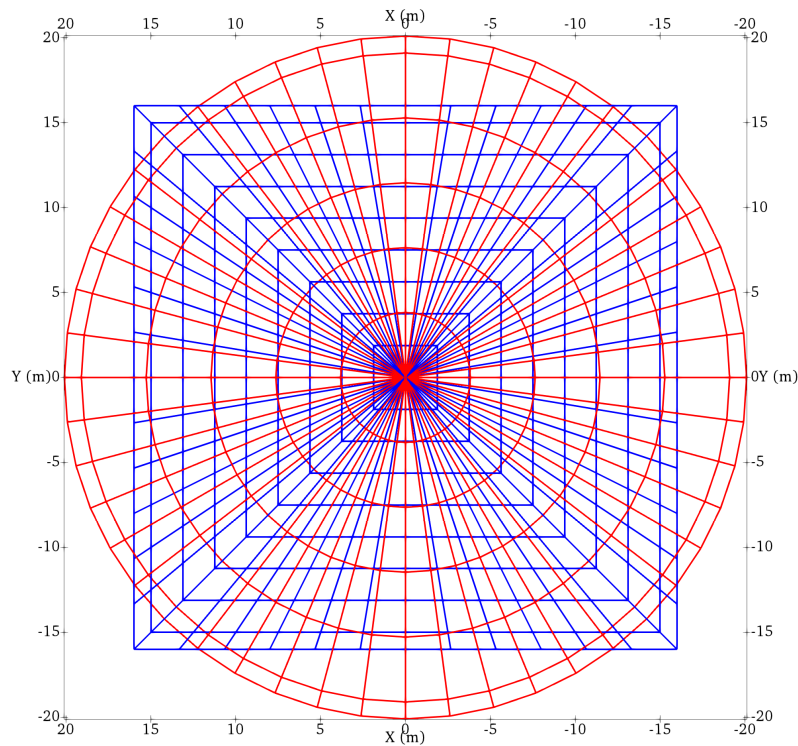
Figure 22. Top view comparison of the two fish cage shapes at their initial state, prior to exposure of the flow velocity, where $C = 120$ m, $H = 20$ m, $W = 60$ kg/m.

4.1.2. Drag forces for different circumferences

This section discusses how different circumferences affect the drag force on the fish cages. Figure 23 shows the drag force exerted on both fish cages for increasing circumferences. The polynomial fittings, plotted using dashed lines in Figure 23, have different polynomial functions for the different current velocities. These functions are presented in Table 3.

When the two fish cage models have the same design height, are equally weighted and are subjected to the same velocity, the squared cage experiences a larger drag force than the circular cage for all the different circumferences. Additionally, the drag force on the fish cages increases almost linearly with varying circumferences under different flow velocities. The deficit between the drag force exerted on the fish cages is increased with different circumferences, where the drag force increases obliquely upwards with the flow velocity. When the circumference of a fish cage is increased, a greater proportion of nettings affiliate the fish cage, and thus more structural

blockage is present. The additional structural blockage of nettings causes a larger drag force on both fish cages.

In practice, the current velocity is not acting perpendicular to most of the nettings, as previously presented in Figure 19. The inflow angle θ of the net-panel element, *i.e.*, the angle between e_n and U_c in Figure 7, has a significant impact on the drag force exerted on the fish cages. Figure 24 illustrates the circular cage with different circumferences, where the design height, weight and incoming flow velocity are the same. When the fish cages are subjected to smaller current velocities, the angle between e_n and U_c is greater for smaller circumferences, and thus the nettings act more perpendicular towards the current velocity. Hence, the increase of the circumference of the fish cages results in minor difference of the drag force exerted on the fish cages, when the fish cages are subjected to smaller velocities.
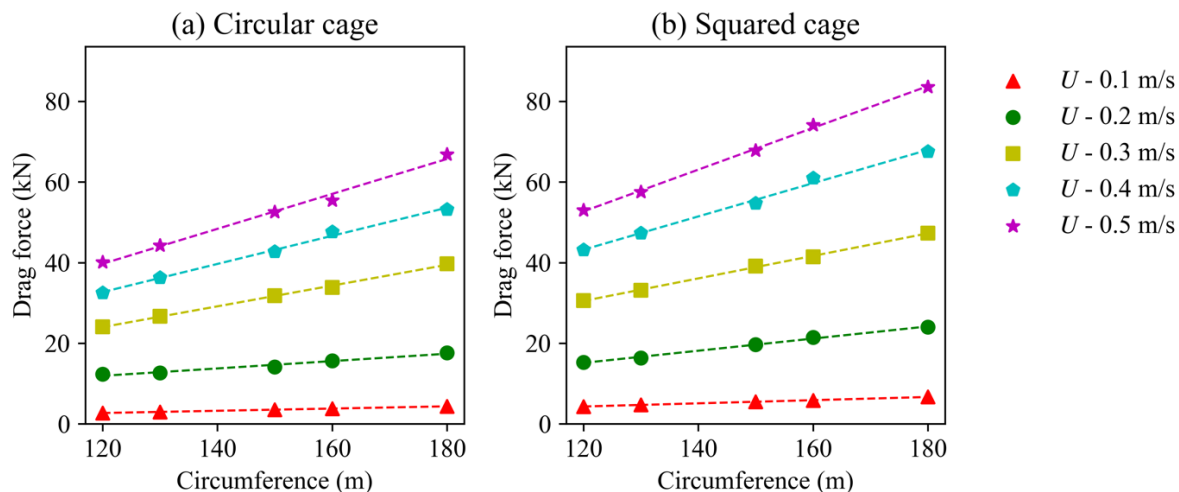
Figure 23. Comparison of the drag forces on the fish cages for different circumferences and velocities, where $H = 20$ m and $W = 40$ kg/m. The dashed lines are the polynomial fittings.

Table 3. Polynomial functions for the drag force on the fish cages for different circumferences and current velocities, where $H = 20$ m and $W = 40$ kg/m.

	Fish cage	
Current velocity (m/s)	Circular	Squared
0.1	$F_D = 0.02759\,C - 0.6056$	$F_D = 0.03934\,C - 0.4051$
0.2	$F_D = 0.09122\,C + 0.9838$	$F_D = 0.1507\,C - 2.942$
0.3	$F_D = 0.2573\,C - 6.871$	$F_D = 0.2793\,C - 3.025$
0.4	$F_D = 0.3489\,C - 0.0178$	$F_D = 0.4126\,C - 6.317$
0.5	$F_D = 0.4335\,C - 12.32$	$F_D = 0.518\,C - 9.47$
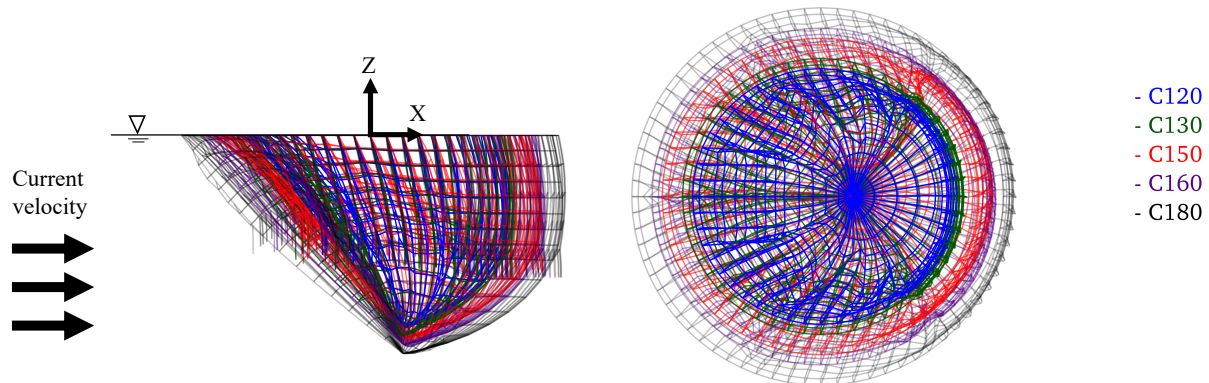
Figure 24. Illustration of different circumferences for the circular cage, where $H = 20$ m, $W = 40$ kg/m and $U = 0.3$ m/s.

4.1.3. Drag forces for different design heights

The two previous sections discussed how the drag force on the fish cages was affected by different current velocities and circumferences. In this section, a comparison of the drag force exerted on the fish cages is discussed for varying design heights.

An illustration of the drag force for different design heights with different circumferences is presented in Figure 25. Overall, an increase of the design height results in larger drag forces on both fish cages, where the squared cage experiences a larger drag force than the circular cage, given the same circumference, weight and current velocity. When the design height of the two fish cages is increased, the resulting drag force on the fish cages is more linearly increased for the squared cage than for the circular cage, given that the fish cages have the same circumference, weight and current velocity. This linearity occurs with the shape deformations, as aforementioned at the start of Section 4, where the squared cage sustains its shape greater than the circular cage for strong flow velocities.
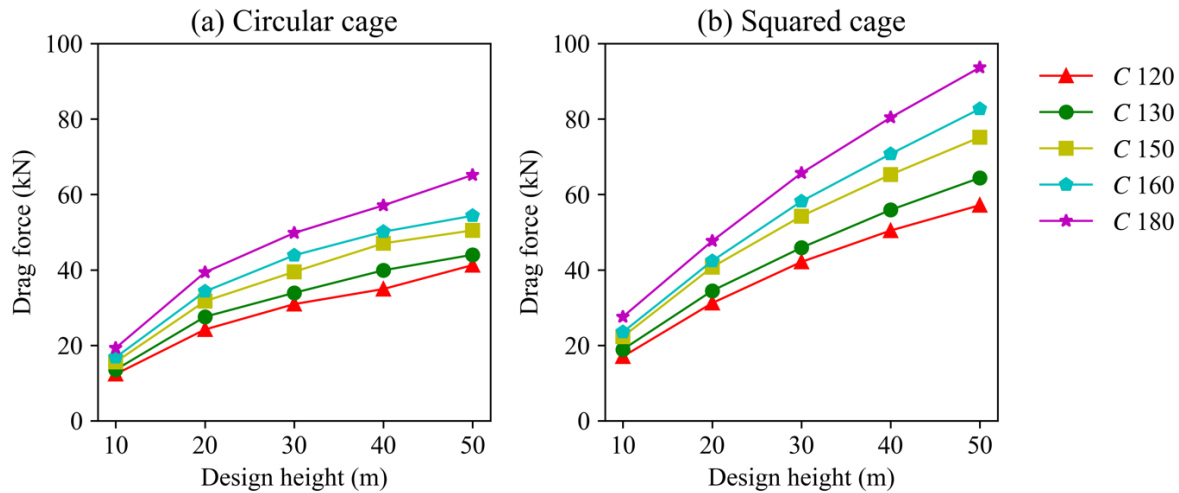
Figure 25. Comparison of the drag forces on the two fish cage models for different design heights and varying circumferences, where $W = 50$ kg/m and $U = 0.3$ m/s.

Figure 26 shows the drag force on the two fish cages under different current velocities for varying design heights, with the same circumference and weight. The polynomial functions, plotted using dashed lines from Figure 26, are presented in Table 4. Correspondingly, when the fish cages have large design heights and are subjected to strong current velocities, the fish cages drift further with the current and the downstream nettings moves obliquely upwards in the current direction. Hence, the drag force exerted on the fish cages becomes very similar for the largest design heights, when they are exposed to the same current velocity. In addition, the deficit between the resulting drag force on the squared fish cage for different design height is greater for the squared cage than for the circular cage, given the same dimensions, weight and current velocity.

Fish cages with large design heights experience a similar deformation for increased velocities as the illustrations in Figure 18, 19 and 20. However, the downstream nettings tend to drift further in the current direction for fish cages with larger design heights compared to smaller design heights as illustrated in Figure 27.
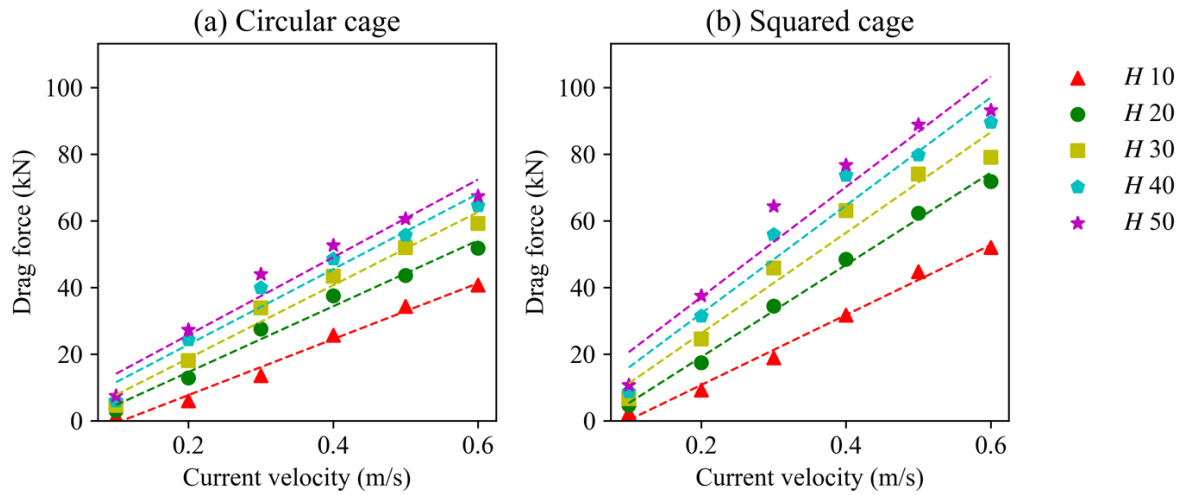
Figure 26. Comparison of the drag force on the two fish cage models subjected to increasing current velocities with varying design heights. The dashed lines are the polynomial fittings, where $C = 130$ m and $W = 50$ kg/m for both fish cages.

Table 4. Polynomial functions for the drag force on the fish cages under different current velocities and design heights, where $C = 130$ m and $W = 50$ kg/m.

| Design height (m) | Fish cage | |
	Circular	Squared
10	$F_D = 83.91\ U - 9.065$	$F_D = 105\ U - 10.15$
20	$F_D = 98.79\ U - 5.158$	$F_D = 138.3\ U - 8.523$
30	$F_D = 109.7\ U - 3.197$	$F_D = 150.7\ U - 3.876$
40	$F_D = 113.1\ U + 0.2485$	$F_D = 162\ U - 0.1962$
50	$F_D = 116.6\ U + 2.447$	$F_D = 165.3\ U - 4.063$
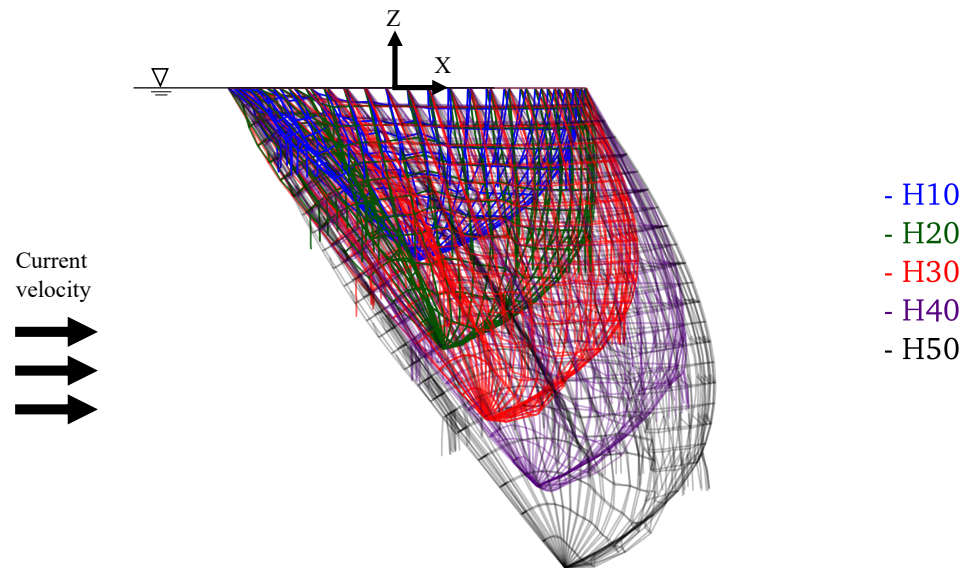
Figure 27. Illustration of the different design heights for the circular cage, where $C = 130$ m, $W = 50$ kg/m and $U = 0.3$ m/s.

4.1.4. Drag forces for different weights

The drag force on the fish cages is influenced by different dimensions and flow velocities, as previously discussed in Section 4.1.1 to 4.1.3. In this section, a comparison of the drag force on the fish cages for different weights is carried out.

Figure 28 shows the drag force exerted on both fish cages for different weights with varying circumferences, where the continuous and dashed lines refer to the flow velocities 0.2 m/s and 0.5 m/s, respectively. The numerical results indicate different responses between the drag force exerted on the two fish cages when various weights are applied, and the fish cages have the same dimensions and are subjected to the same current velocity. The squared cage experiences the smallest and largest drag forces for 40 kg/m and 70 kg/m, respectively, while the drag force exerted on the circular cage alternates for the different weights, given the same dimensions for a current velocity of 0.5 m/s. However, the weights result in different drag forces on the squared cage only when the current velocities are greater than 0.3 m/s. As seen in Figure 28, when the fish cages are subjected to a small current velocity (continuous lines), the deficit between drag force on the fish cages for the smallest and greatest weight is very small. For these small velocities, the smallest weight is sufficient.

In practice, the weight applied on a fish cage depend on the material of the net, fish cage size and cost. In addition, the weight system provides adjacent support of the fish cage nettings in order to mitigate cage deformation when the fish cage is subjected to the current velocity. Typically, heavier weights applied to a fish cage induce a greater drag force on the fish cage. However, the circular cage experiences almost the same drag forces for all the weights, given the same dimensions. This ensues from the cage deformation of the circular cage for strong flow velocities, where the nettings of the circular cage elongate in the current direction and are compressed towards the centre of the cage, independent of the total weight. Hence, the drag force exerted on the circular fish cage is similar for most cases with different weights, given the same dimensions. The significant cage deformations indicate that the weight applied on the circular fish cage is not sufficient and that a different weight system, *e.g.,* a bottom collar, may be more suitable for fish cages with circular shapes.
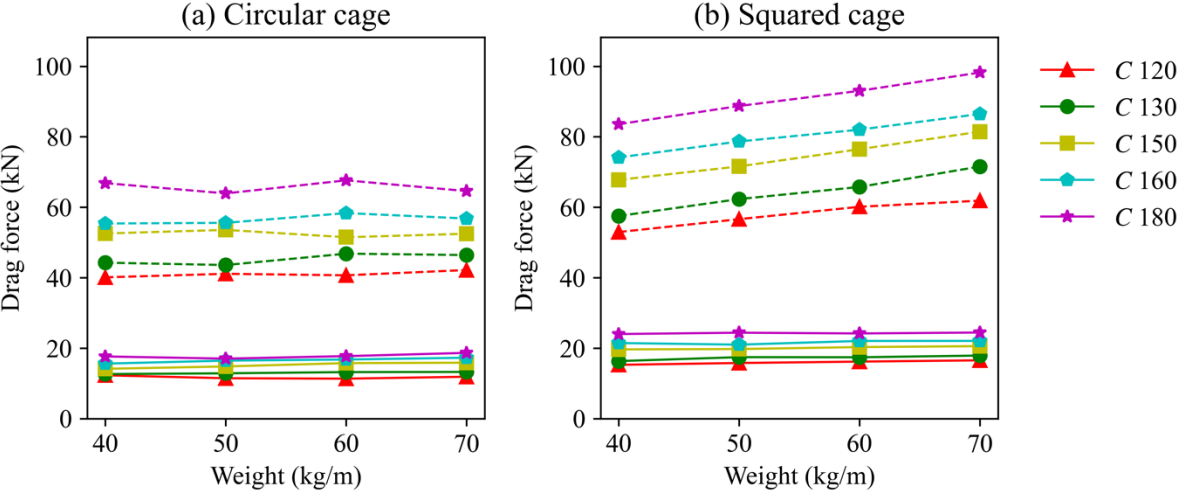
Figure 28. Comparison of the drag force on the fish cages for different weights and varying circumferences. The fish cages have $H = 20$ m, and the continuous and dashed lines refer to $U = 0.2$ m/s and 0.5 m/s, respectively.

4.1.5. Normalised drag forces

In addition to the drag force, two normalised drag relations are compared and are obtained as:

$$F_{n,1} = \frac{F_d}{gCW} \tag{37}$$

$$F_{n,2} = \frac{F_d}{\frac{1}{2}C_d\rho H \frac{C}{\pi} u^2} \tag{38}$$

where F_d is the drag force from numerical results and C_d is the drag coefficient. The value of C_d is estimated as 0.37 based on Eqs. (19)-(25), proposed by Kristiansen and Faltinsen (2012).

The first normalised equation (37) is proposed in this study to compare the drag force on the fish cages for the weight, as gCW is the total weight on a fish cage. The second normalised equation (38) is implemented in this study in order to compare the drag force exerted on the fish cages for the different dimensions and current velocities, as the denominator represents the respected equation to calculate the drag force on a fish cage.

Figure 29 presents the normalised drag forces for both fish cages with multiple circumferences and weights for different current velocities, given the same design height. Eq. (37) obtains ascending normalised drag forces on the fish cages by increasing the current velocities, while Eq. (38) obtain descending normalised drag forces on the fish cages with increasing current velocities.

In general, the squared cage produces larger $F_{n,1}$ and $F_{n,2}$ compared to the circular cage, as seen in Figure 29. In Figure 29 (a), it can be observed that the current velocity has an important influence on the resulting normalised drag force, where an increase of the velocity causes a larger normalised drag on both fish cages. In comparison, as seen in Figure 29 (b), the normalised drag is decreased when the current velocity is increased, where the normalised drag force is greater for the squared cage than the circular cage. Since Figure 29 (b) is based on the dimensions of the fish cage, and the squared fish cage sustain its shape greater than the circular cage for small current

velocities, the normalised drag force is larger for the squared cage than the circular cage. When both fish cage models are exposed to strong current velocities, they both experience large deformations, and thus similar normalised drag forces exerted on the fish cages.
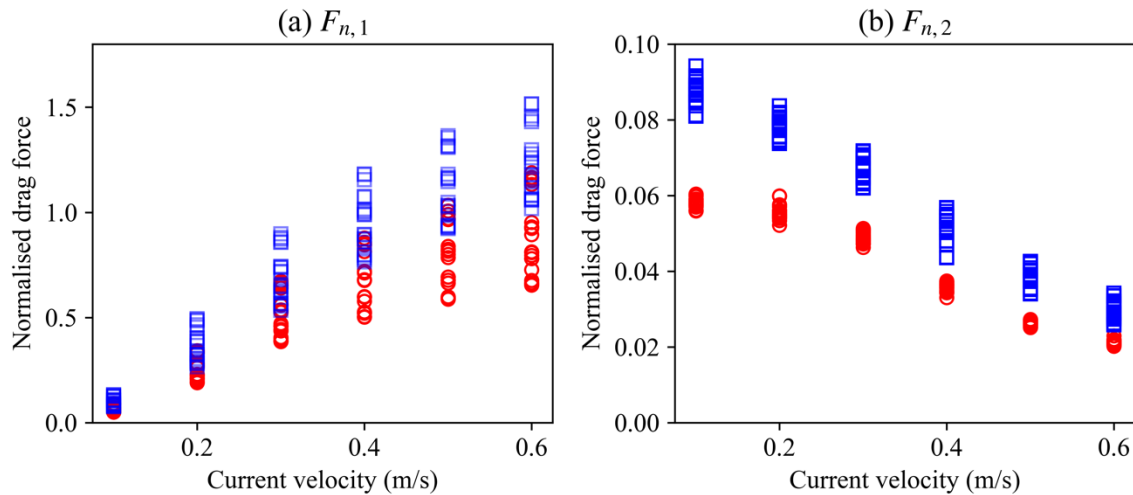
Figure 29. Relationship between normalised drag forces on the fish cages for different current velocities. $F_{n,1}$ is based on different circumferences and weights, while $F_{n,2}$ is obtained from different circumferences where $H = 30$ m. The squared and circular cages refer to the blue squares and red circles, respectively.

4.1.6. Normalised drag force per unit volume

In Section 4.1.1 to 4.1.5, the drag force on the fish cages was solely measured against different dimensions, weights and flow velocities. An additional study of the drag force per unit volume is discussion in the following section to compare the correlation between the drag force on the fish cages with respect to the cultivation volume of the fish cages. Since the second normalised drag force $F_{n,2}$ is descending for increasing current velocities, Eq. (37) is chosen for comparing the drag force on the fish cages against the cultivation volume.

An illustration of the drag per unit volume with different design heights is presented in Figure 30. In general, the squared cage indicates a larger drag per unit volume, which agree with previous discussion regarding compression of the fish cage nettings in Section 4.1.2. The characteristics of the two models are different, where the circular cage experience a greater cage deformation but produces a smaller drag force than the squared fish cage.
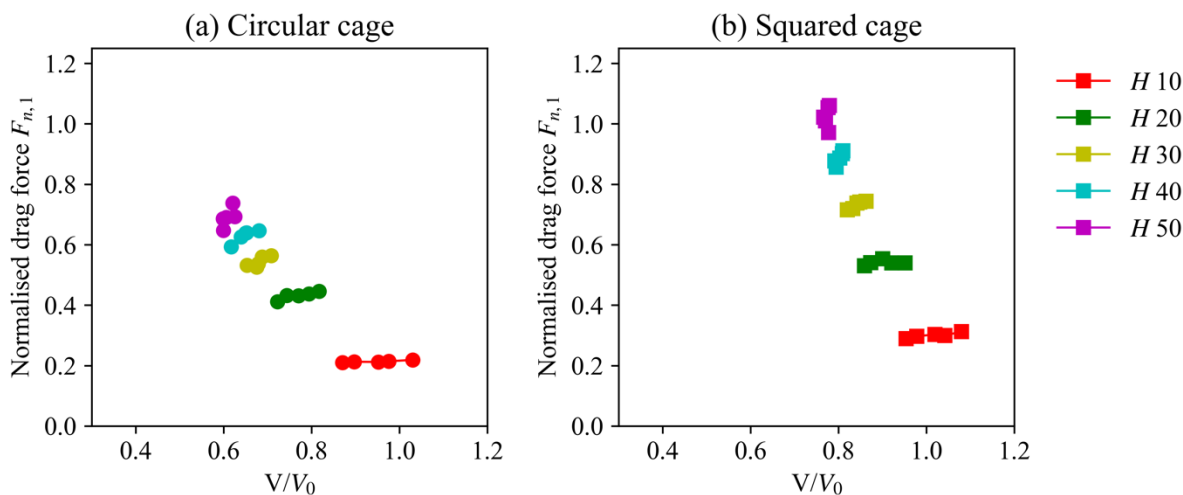
Figure 30. Illustration of the normalised drag force $F_{n,1}$ per unit volume for varying design heights, where $W = 50$ kg/m and $U = 0.3$ m/s. The different scattered dots for the same colour refer to increasing circumferences (left to right/bottom to top).

4.2. Cultivation volume

4.2.1. Volumes under different current velocities

In this section, the cultivation volume of the fish cages is discussed when the fish cages are subjected to different current velocities. Figure 31 shows the volume factor of the two fish cages for different current velocities with varying design heights (horizontal) and circumferences (vertical). When the current velocity subjected to both fish cages is small, both fish cages experience a minor deviation with respect to the initial volume. As aforementioned in Section 3.2.2, the supplementary weight applied on the fish cages to mitigate the net deformation is not included at the start of the simulation process, which induce a larger volume compared to the initial fish cage volume, and thus $\frac{V}{V_0} > 1$.

As aforementioned discussed in Section 4.1.1, the bottom nettings of both fish cages tend to drift such that the downstream end displace obliquely upwards in compliance with the current velocity. In addition, the circular fish cage experiences a larger deformation of the nettings compared to the squared cage, which, for strong flow velocities, results in displacement of the nettings towards the centre of the cage. Hence, larger flow velocities induce a smaller volume factor for the circular cage compared to the squared cage, as seen in Figure 31.

43
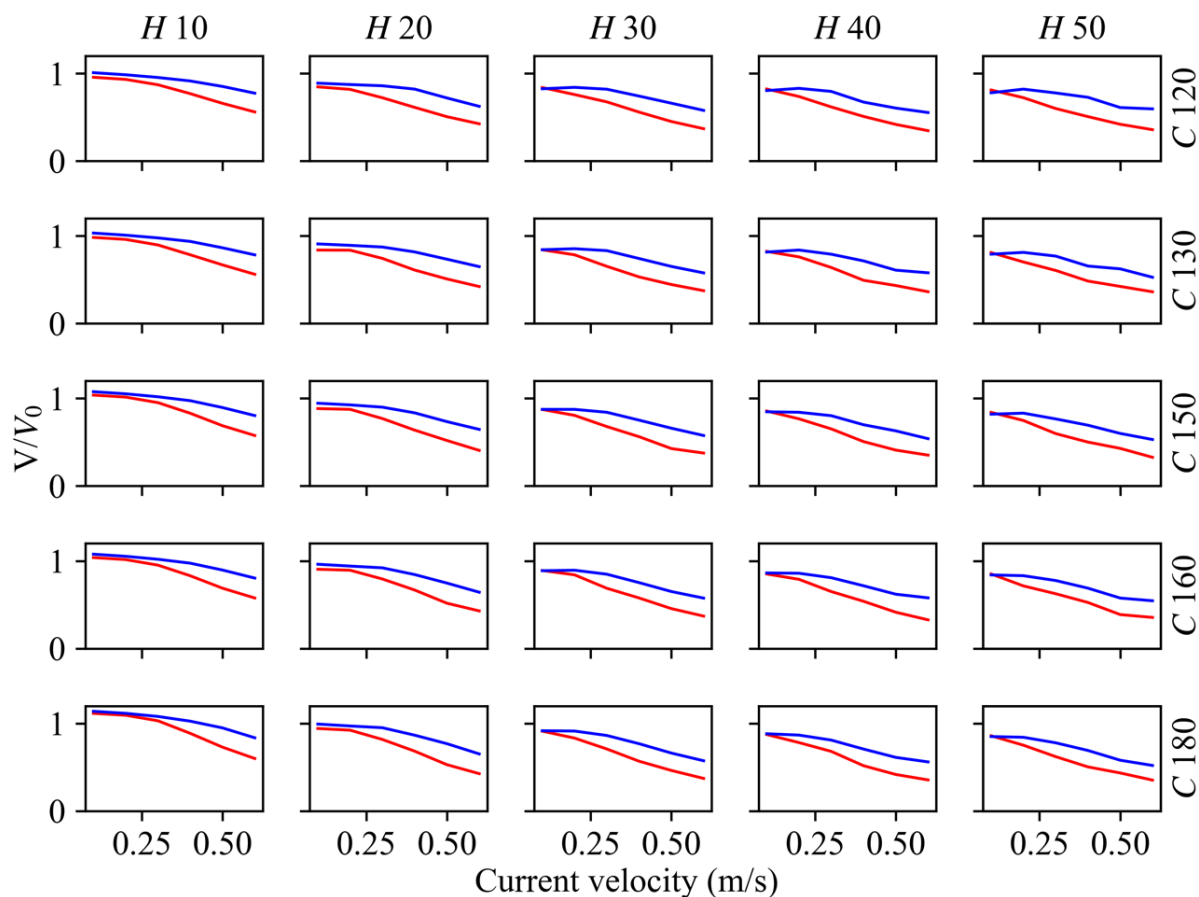
Figure 31. Illustration of the volume factor of the two fish cages with $W = 50$ kg/m, and different current velocities design heights and circumferences. The red and blue lines refer to circular and squared cage, respectively.

Figure 32 shows the total cultivation volume of both models for different current velocities with varying circumferences. Overall, increasing current velocities induce decreasing cultivation volumes for both fish cages. When $U < 0.4$ m/s, the smallest and largest cultivation volumes ensue from the squared and circular cage, respectively. This agree with previous discussion at the start of Section 4, where the circular fish cage experiences a larger shift in the current direction than the squared cage, and the nettings are narrowed towards the centre of the cage, causing a smaller cultivation volume. Comparatively, the squared cage succeeds in retaining its shape greater than the circular cage, for increasing flow velocities, which induce a larger cultivation volume for the squared cage.

The descending cultivation volume for large current velocities reduces the living space for the fish due to large cage deformations. Consequently, it is critical to assess the net volume

reduction for the environmental impacts at the fish farming site. In general, the circular cage has a larger volume than the squared cage within the recommended velocity range for salmon, *i.e.,* 0.2-0.5 m/s.
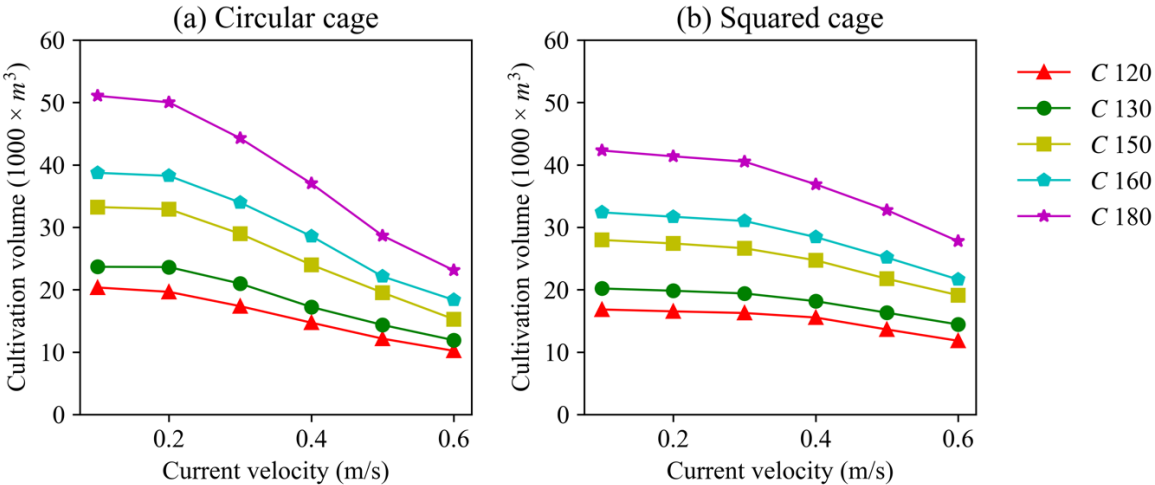
Figure 32. Comparison of the cultivation volume under different current velocities for varying circumferences, where $H = 20$ m and $W = 50$ kg/m.

4.2.2. Volumes for different circumferences

This section contains a discussion of how the different circumferences influence the cultivation volume of the fish cages. Figure 33 presents the volume factor of both fish cages for varying circumferences, when they have the same design height, weight and velocity. Overall, both fish cages experience an increase of the volume factor by increasing the circumference. In general, the circular cage incorporates a larger cultivation volume than the squared cage, given the same circumference of the fish cage. In contrast, the volume factor of the circular cage is smaller than the squared fish cage, given the same design height, weight and flow velocity. The difference in volume factors for the two fish cages ensue from the characteristic cage deformations, where the circular fish cage deforms more than the squared cage, given same dimensions, weight and current velocity.
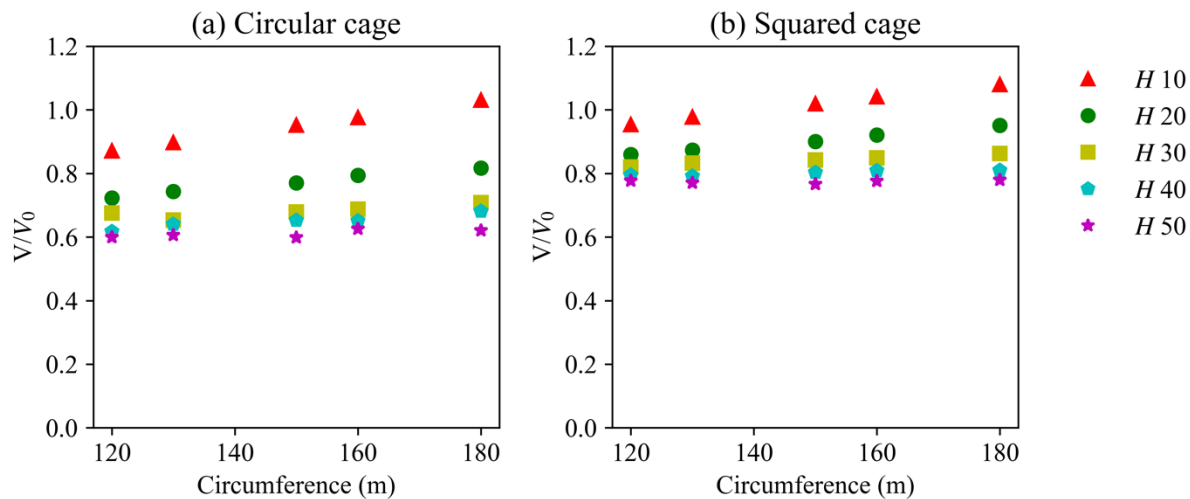
Figure 33. Comparison of the volume factor for different circumferences with varying design heights, where $W = 50$ kg/m and $U = 0.3$ m/s.

4.2.3. Volumes for different design heights

In the present section, an explicit comparison of the fish cage volume of the two fish cages for different design heights is discussed. A comparison of the volume factor for varying design heights with different circumferences is presented in Figure 34. The volume factor is to a large extent affected by different design heights, where the circular cage predominantly experiences a smaller volume factor than the squared cage, given the same circumference, weight and current velocity. The shortest design height results in the greatest volume factor, for both fish cages. This ensues from the weight applied to the fish cages, where the sinker weights on fish cages with small design heights affiliates a smaller quantity of netting than for fish cages with larger design heights. In addition, as aforementioned in Section 4.1.3, the bottom nettings of both fish cages tend to drift such that the downstream netting displaces obliquely upwards with the current velocity. This drift and deformation occur to a greater extend for the circular cage, which causes the volume factor to be smaller for the circular cage than for the squared cage.

When the design height is increased, the discrepancy between the volume of the two cages is very similar, when the fish cages have the same dimensions, weight and is subjected to a current velocity of 0.3 m/s. This is presented in Table 5, where the smallest discrepancy occurs when the fish cages have a design height of 30 m.

Since the cost of netting is directly correlated to the fish cage shape, shorter design heights are more expedient and would reduce the overall cost of a fish farm. The overall cost includes inspection time and repairing of the net and/or replacement within a time period. While a reduced cost benefits an aquacultural company, the fish's welfare is of equal importance. Typical fish cages are limited to a certain amount of fish to be located within the cage. The size of the fish species needs to be ascertained in order to assure welfare of the fish, which can be set as a minimum kilogram of the fish per cubic meter. For shorter fish cages, the number of fish that can be sectioned within the cage is limited, while larges fish cages have the possibility of breeding more fish.

Previous discussion shows that the largest circumference results in the greatest volume factor. By incorporating the discussion of the volume factor for different design heights, the preeminent fish cage would comprise of a design height of 10 m with a circumference of 180 m. When the design heights of the fish cages are as short as 10 m, the fish cages tend to remain in its original position on the contrary to larger fish cages, which are elongated in the current direction.
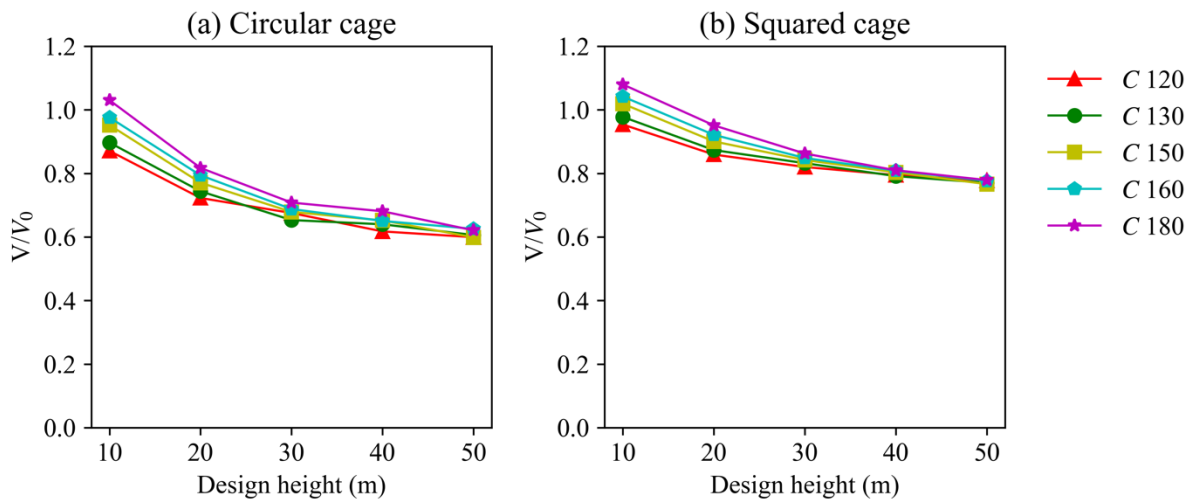
Figure 34. Illustration of the correlation between the volume factor and design height for varying circumferences, where $W = 50$ kg/m and $U = 0.3$ m/s.

Table 5. Comparison of the cultivation volume for different design heights, where $C = 130$ m, $W = 40$ kg/m and $U = 0.3$ m/s.

Design height (m)		10	20	30	40	50
Cultivation volume (1000 × m³)	Circular cage	13.1	20.4	26.9	34.7	40.7
	Squared cage	11.3	19.1	26.8	34.0	41.7

4.2.4. Volumes for different weights

The cultivation volume of the two fish cage models for different weights is discussion in this section. Figure 35 and 36 shows the volume factor for different weights with varying circumferences and design heights, respectively. Both figures reveal a similar pattern, where larger weights cause minor difference regarding the volume factor. The results indicate that the volume factor is slightly increased for most cases, where the squared fish cage experiences a larger volume factor for all weights than the circular fish cage, given the same dimensions and current velocity.

In practice, the type of weight system selected to mitigate the cage deformation is dependent on environmental conditions and the shape of the fish cage. Since the netting of sea-based fish cages are made of polymer, the weight needs to be of adequate mass in order to prevent cage deformation and light enough to prevent wear and tear of the net. The minor difference of the volume factor for different weights indicates that the largest weight dispersed on both fish cages is redundant, since the smallest weight provide a similar volume factor, given the same dimensions and current velocity. However, under the same dimensions, the nettings on the circular fish cage deform significantly more than the nettings of the squared cage for strong current velocities. This implies that the weight system applied to the circular fish cage is not sufficient.
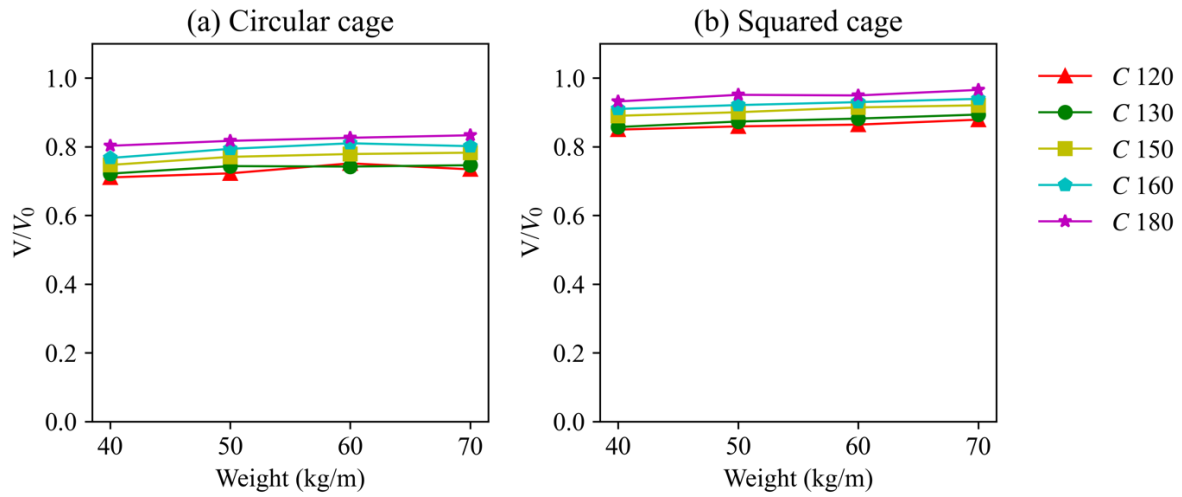
Figure 35. Comparison of the volume factor for different weights with separate circumferences, where $W = 20$ m $U = 0.3$ m/s.
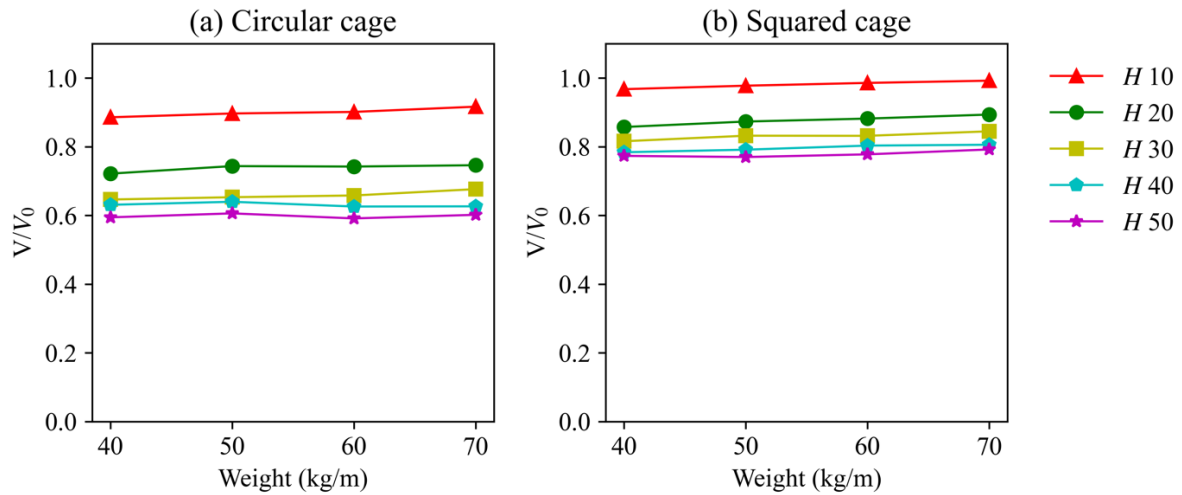
Figure 36. Comparison of the volume factor for different weights with respect to increased design heights, where $C = 130$ m and $U = 0.3$ m/s.

4.2.5. Cultivation volume per netting area

The most prominent difference of the two fish cage models is the overall area of netting. As previously discussed, the shapes of both cages result in different drag forces and cultivation volumes, given the same dimensions, weight and flow velocity. In order to evaluate the relative difference of cultivation volume per netting area for the two fish cages, the total culmination volume and volume factor are measured against the area of netting of the two fish cages in this section.

Figure 37 shows the cultivation volume for different area of netting with varying design heights. The total netting area is significantly smaller for the squared cage than for the circular cage, which, in practice, reduces the overall cost for production and replacement of the nettings. Given the same dimensions, weight and velocity, the circular cage contains a larger total cultivation volume for smaller current velocities, while the squared fish cage has a larger volume per area of netting. As fish cages are gradually increased in order to produce more fish, the total volume is a considerable factor when designing fish cages.

A comparison of the volume factor for different area of netting with varying design heights, is presented in Figure 38. The squared cage experiences a larger volume factor than the circular cage for a smaller proportion of netting area, given the same circumference, weight and flow velocity. The scattered dots for the circular cage in Figure 38 (a) are wider spread than for the squared cage in Figure 38 (b), which ensues from the characteristic cage shapes illustrated in Figure 22. Hence, the area of netting increases significantly more for the circular cage than for the squared cage, when the design height is increased.

The squared fish cage shape produces larger volumes and volume factors per netting area compared to the circular fish cage and is therefore the dominant fish cage. Correspondingly, the squared fish cage uses a smaller portion of area at the water surface (floating collar) with respect to an entire fish farm than the circular cage, as previously presented in Figure 22.

Figure 37. Comparison of the cultivation volume for different areas of netting. The scattered dots have different circumferences, increasing from left to right, where $W = 50$ kg/m and $U = 0.3$ m/s.
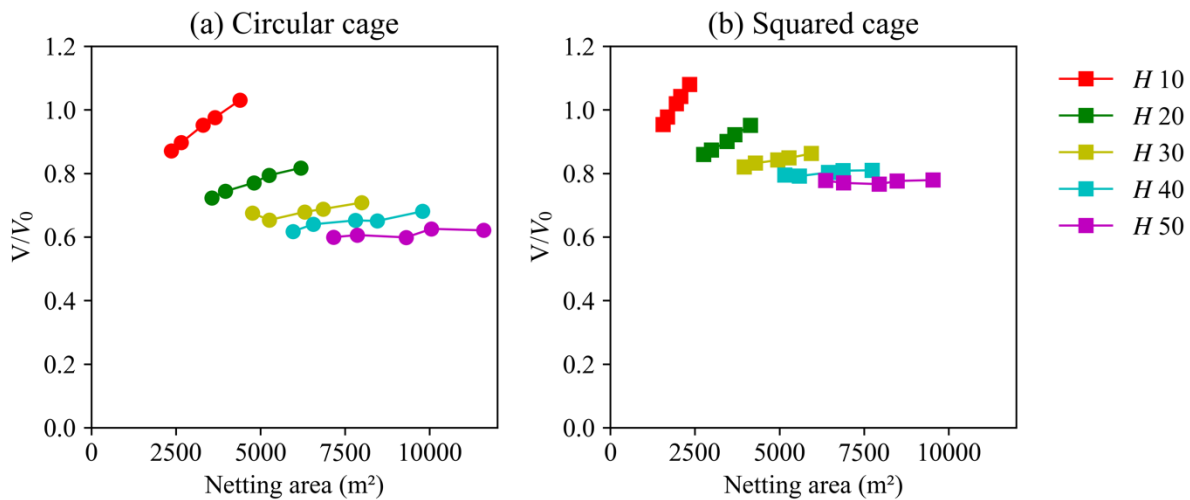
Figure 38. Comparison of the volume factor for different areas of netting. The scattered dots have different circumferences, increasing from left to right, where $W = 50$ kg/m and $U = 0.3$ m/s.
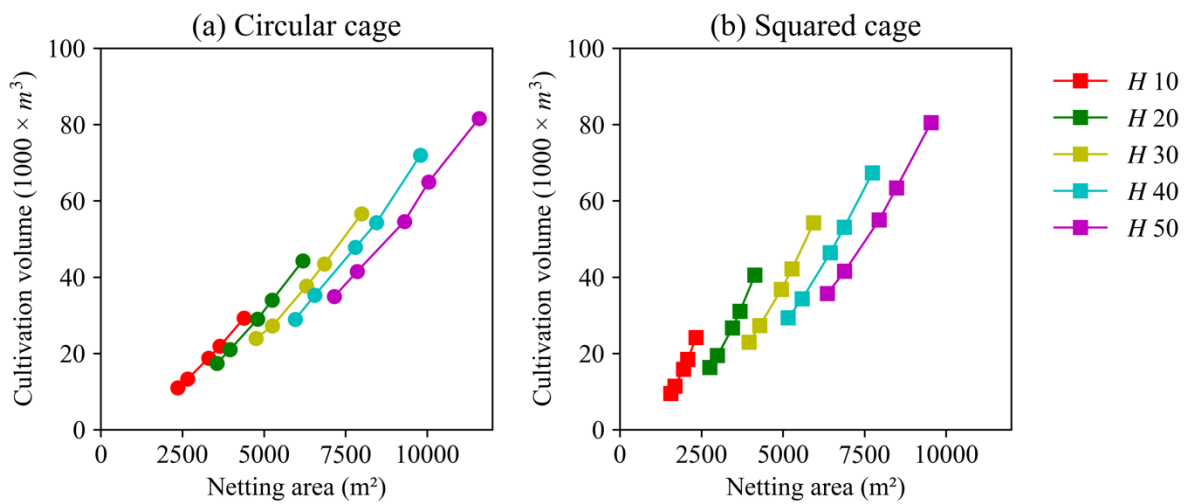
4.3. Fish cage height

4.3.1. Fish cage heights under different current velocities

This section compares the fish cage heights of the two fish cages under different current velocities. Figure 39 shows the fish cage height under different current velocities for varying design heights and circumferences. In general, an increase of the current velocity results in a shorter fish cage height for both fish cages. The circular cage has a larger height than the squared cage for current velocities smaller than 0.4 m/s, given the same dimensions and weight.

The fish cage height of the two fish cage models, with $H < 40$ m, gradually converges towards the same fish cage heights for increasing current velocities. In practice, the fish cage height is included as a measurement for comparison during the design phase of fish cages, as the distinction in fish cage height may influence the design of feeding tubes and similar operations regarding the net.

When the current velocity is increased, the downstream netting on both models undergo a shift obliquely upwards in the flow direction, which causes a reduction of the measured fish cage height. In addition, for large dimensions and velocities, the squared fish cage experiences an upwards shift of the downstream bottom netting, which lifts one side of the bottom netting, leaving the other side of the bottom netting further down. The downstream nettings are shifted from left to right in a characteristic pattern. As the fish cage height is measured as the distance that joins the highest node with the lowest node, the fluctuating pattern of the bottom netting for the squared cage results in the largest fish cage height for the strongest current velocities. This fluctuation is illustrated in Figure 40.

Figure 41 presents the discrepancy between the fish cage heights for the two models. The figure reveals that the height of the two fish cages is directly correlated their shapes, where the circular cage, in general, possesses a larger fish cage height than the squared cage. When the fish cages are subjected to strong current velocities, the squared fish cage has the largest fish cage height, due to a larger deformation of the circular fish cage than for the squared fish cage.
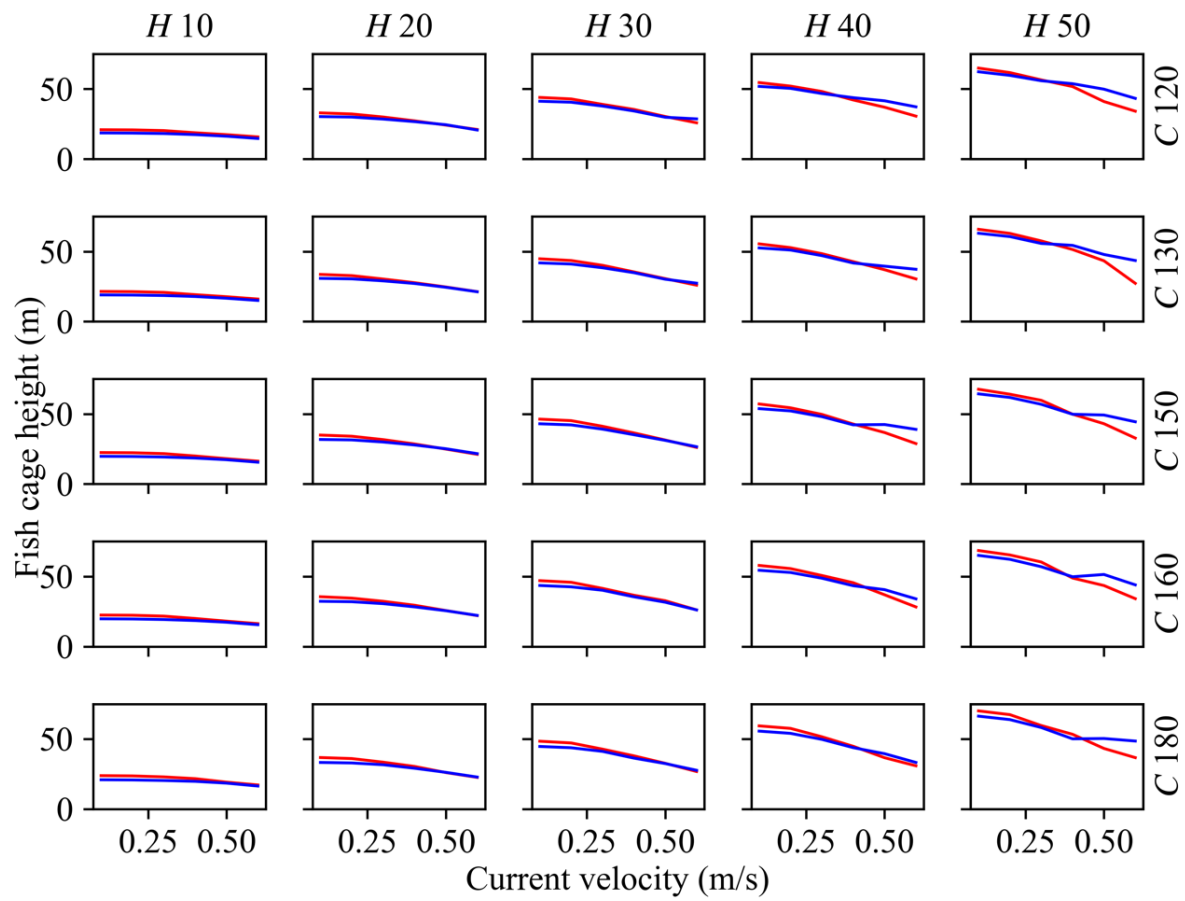
Figure 39. Illustration of the fish cage height for different current velocities with varying design heights and circumferences. The red and blue lines refer to circular and squared cage, respectively, where $W = 50$ kg/m.
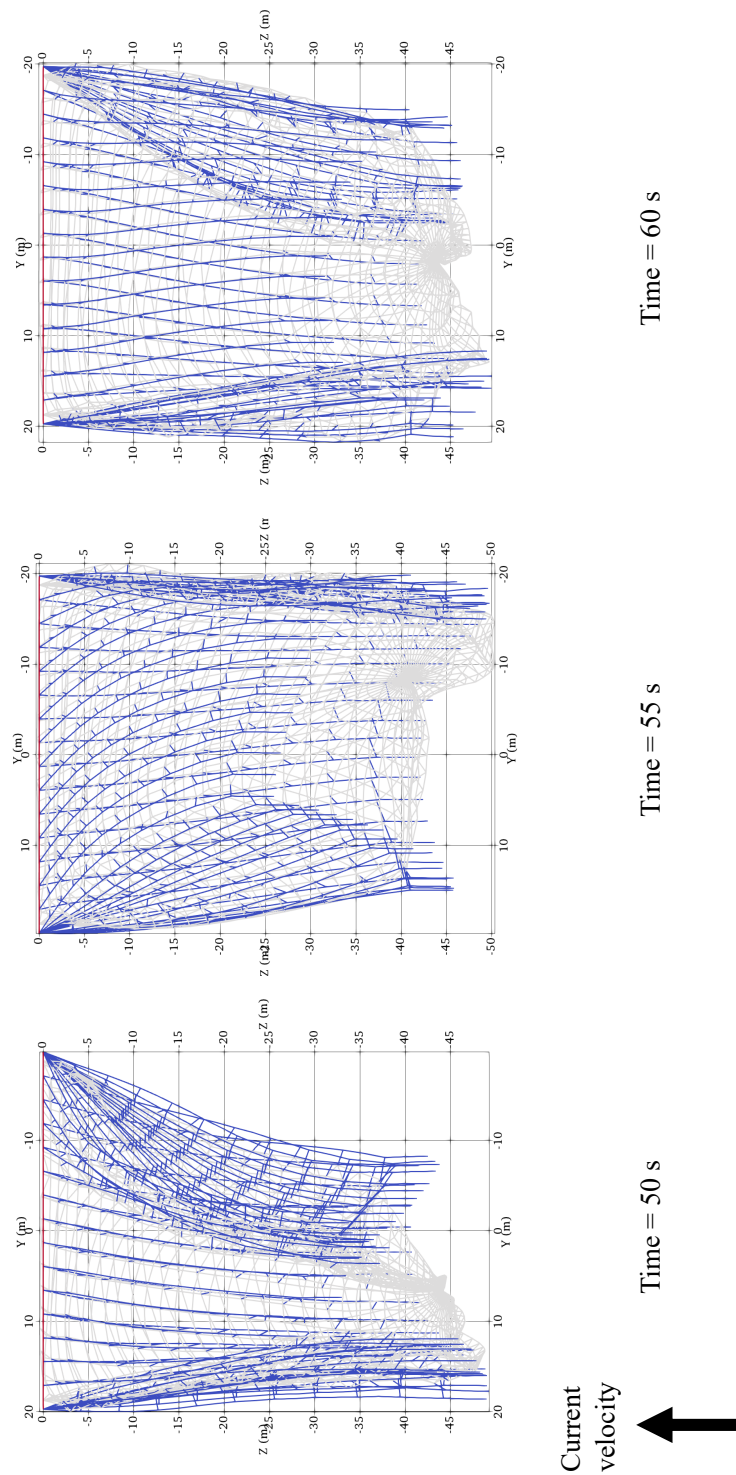
Figure 40. Illustration of the alternating fluctuation of the downstream bottom netting for the squared fish cage, where $C = 150$ m, $H = 50$ m, $W = 50$ kg/m and $U = 0.5$ m/s.
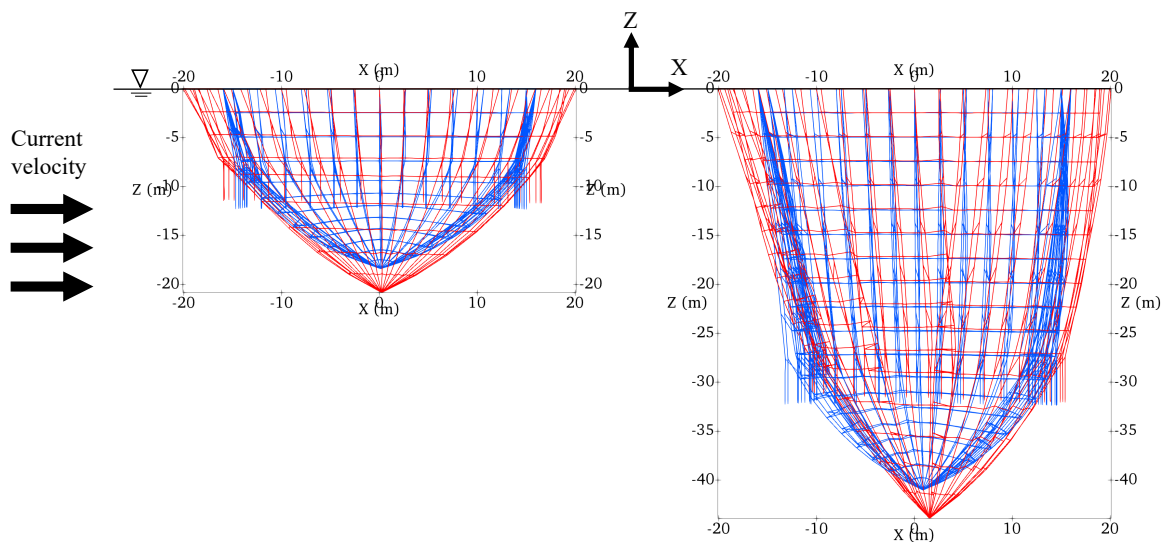
Figure 41. Comparison of the fish cage heights for both fish cages. The red and blue colours represent the circular and squared cage, respectively. The two cages in the left subplot have a design height of 10 m and the two cages in the right subplot have a design height of 30 m, where $C = 120$ m, $W = 60$ kg/m and $U = 0.1$ m/s for all cages.

4.3.2. Fish cage heights for different circumferences, design heights and weights

In this section, a comparison of how the different dimensions and weights influence the fish cage height of the two models is carried out. Figure 42 shows the fish cage height under different current velocities with varying design heights and circumferences. When the design height of both fish cages is increased, the fish cage height increases, as additional nettings affiliates the fish cage. For strong current velocities, the discrepancy of the fish cage height for varying design heights is smaller compared to the discrepancy of these for smaller current velocities.

As aforementioned in Section 4.2.2, the cultivation volume increases in compliance with larger circumferences. Similarly, an increase of the circumference results in a larger fish cage height for both cage models.

The fish cage height for different weights with varying design heights, is illustrated in Figure 43. Similarly, to the discussion of the cultivation volume for different weights in Section 4.2.4, heavier weights contribute small impact on the resulting fish cage heights for smaller current velocities, where the smallest weight of 40 kg/m is more expedient from an economic perspective. As aforementioned in Section 2.3, when the initial weights are added in the simulation process,

the fish cages experience a converging damping motion before it reaches a stable position, where the bouncing no longer affects the length of the fish cage in the vertical direction. Since additional nettings are attached with increasing design heights, smaller fish cages are more affected by the weight added. Hence, fish cages with smaller design heights have a larger deficit between the measured fish cage height and the design height.
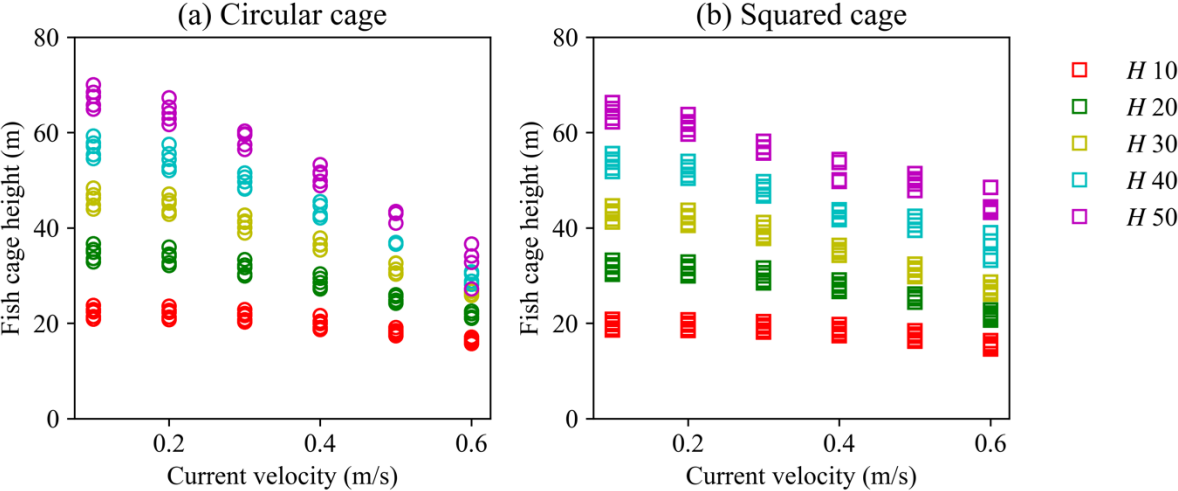
Figure 42. Comparison of fish cage heights with respect to different current velocities, design heights and circumferences, with the same $W = 50$ kg/m.
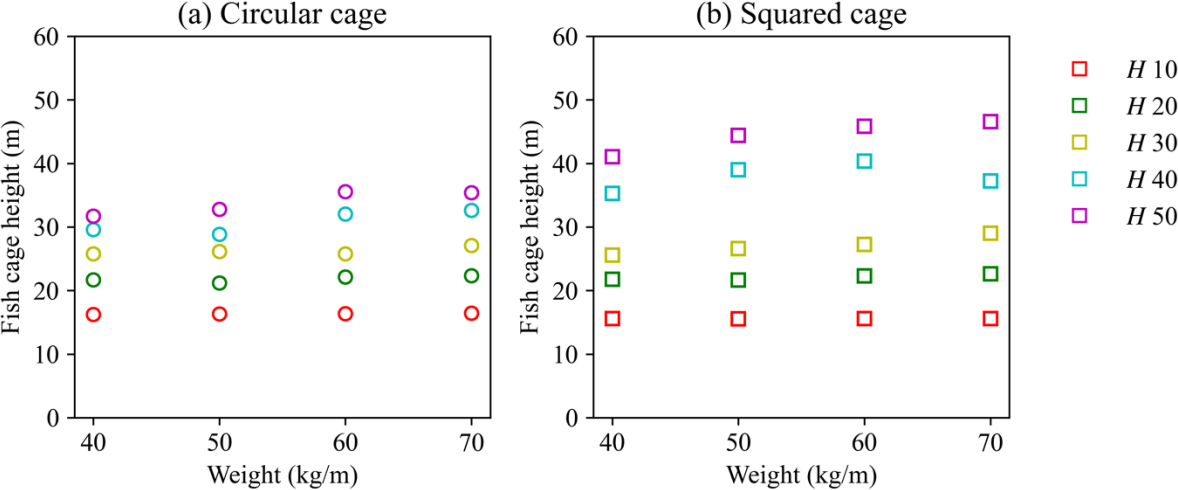
Figure 43. Comparison of the fish cage heights for different weights, where $C = 150$ m and $U = 0.6$ m/s for both cages.

4.4. Cross-section area

4.4.1. Cross-section areas under different current velocities

The present section discusses the cross-section areas of the two fish cages under different current velocities. Figure 44 shows the cross-section area of the two models for increasing current velocities with respect to varying design heights and circumferences. In general, the cross-section area is reduced for increasing current velocities. The circular cage contains a larger cross-section area than the squared cage for velocities smaller than 0.5 m/s, given the same dimensions and weight.

As aforementioned discussed at the start of Section 4, the squared cage sustains the initial cage shape greater than the circular cage, when the fish cages have the same dimensions, weight and are subjected to the same current velocity. As the upwards movement of the bottom nettings is only noticeable for current velocities larger than 0.2 m/s, small discrepancies between the cross-section areas for both cages are measured, when the pure current is increased from 0.1 to 0.2 m/s. When the fish cages are constructed with a design height greater than 30 m, the incoming current velocity induce a greater shift of the downstream netting upwards in the current direction, compared to smaller design heights. As aforementioned discussed in Section 4.3.1, one part of the bottom netting for the squared cage shifts further in the vertical direction than the other part bottom part, for strong current velocities and large design heights. This contributes to a larger cross-section area for the squared fish cage.

Figure 45 shows the cross-section area under different velocities for various design heights. The largest cross-section area occurs for the circular cage, when it is exposed to a velocity of 0.3 m/s and $H > 30$ m, due to elongation of the fish cage in the current direction. The cross-section area is directly correlated to the cultivation volume, and thus critical measurements of the volume are more convenient.
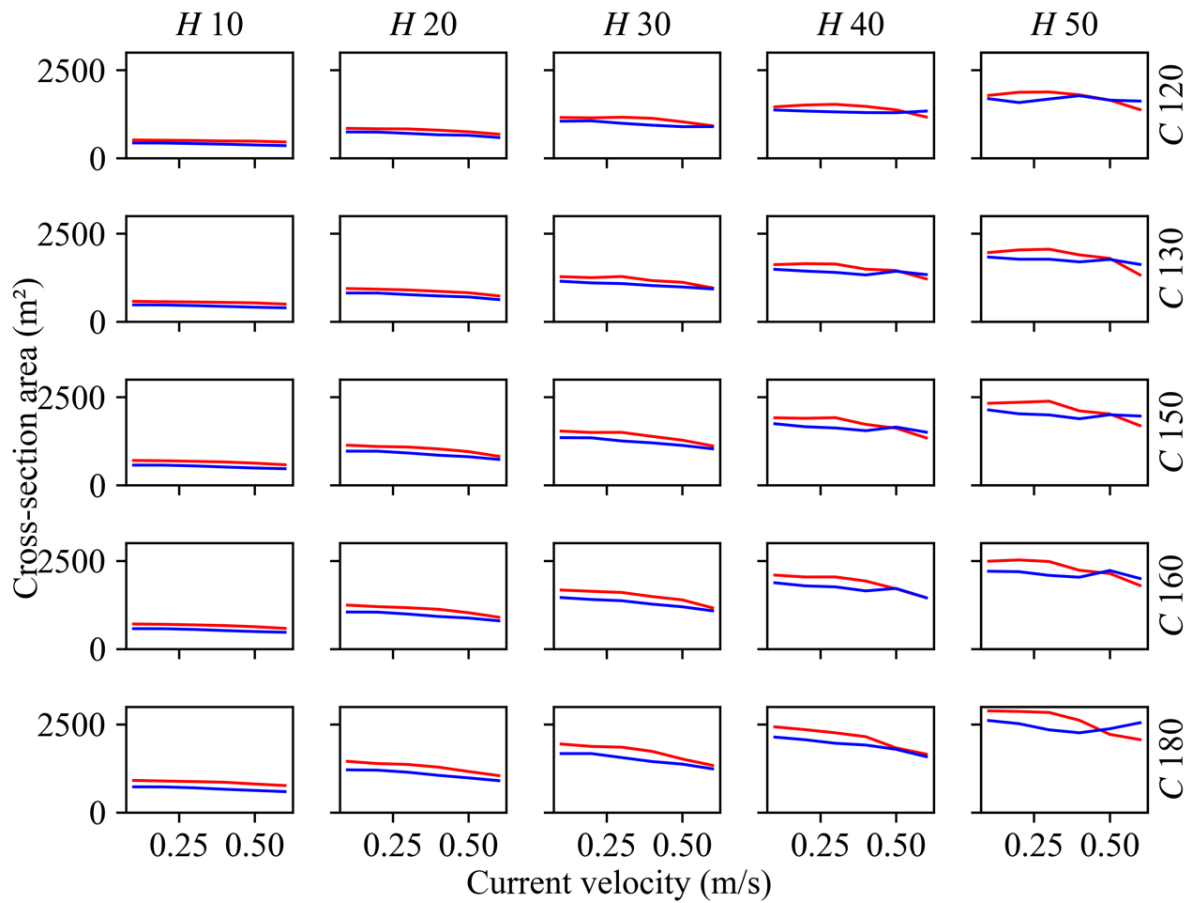
Figure 44. Illustration of the cross-section area of the fish cages for different current velocities with varying design heights and circumferences. The red and blue lines refer to circular and squared cage, respectively, where $W = 50$ kg/m.
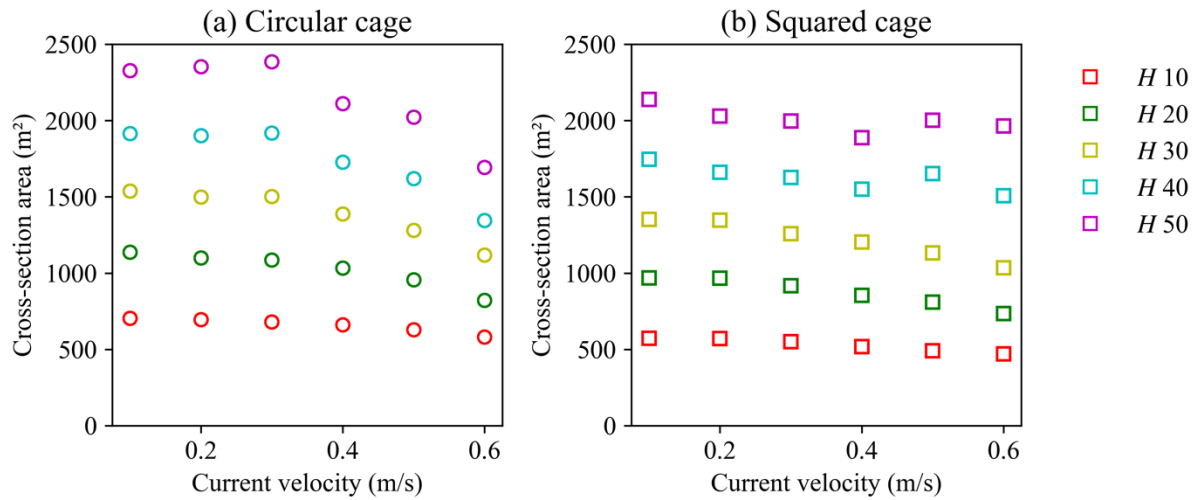
Figure 45. Comparison of the cross-section area subjected to increasing current velocities with varying design heights, where $C = 150$ m and $W = 50$ kg/m.

4.4.2. Cross-section areas for different circumferences, design heights and weights

The previous section discussed the cross-section areas explicitly for different current velocities. In this section, discussions of different dimensions and weights on the cross-section area of the two fish cages are carried out.

The cross-section area for both fish cages increases with larger circumferences, since larger circumferences results in greater area of nettings. In general, the cross-section area is greater for the circular cage than for the squared cage, given the same dimensions, weight and subjected to the same flow velocity. The relative deficits between the cross-section areas of the two fish cages are presented in Table 6, where the deficits between the two models are very similar for increasing circumferences, given the same design height, weight and flow velocity. As the design height is increased, the cross-section area of both fish cages is significantly increased, as seen in Figure 45.

In general, the different weights applied to the fish cages induce a different cross-section area, where the largest weight results in the greatest cross-section area for both cages. However, the different weight results in similar cross-section areas when the fish cages have small dimensions and are subjected to small current velocities.

Table 6. Relative deficit of the cross-section area between the two cages, where $H = 20$ m, $W = 40$ kg/m and $U = 0.3$ m/s.

Circumference (m)	120	130	150	160	180
Relative deficit (%)	18.8	20.4	20.1	20.2	20.7

5. Conclusions and future work

5.1. Conclusions

In this thesis, a comparison study of typical Norwegian gravity-based fish cages is performed in order to investigate the structural responses of fish cages with different dimensions, weights and current velocities.

Both fish cages experience larger drag forces with increased current velocities, design heights and circumferences. The squared cage predominantly experiences a larger drag force than the circular cage, given the same dimensions, weights and velocity. When the current velocity is increased, the squared cage sustains its initial shape greater than the circular cage. Fish cages with large dimensions that are subjected to strong current velocities, experience a large shift obliquely upwards in the flow direction. The circular cage elongates in the current direction, where the netting displaces towards the centre of the cage. The squared cage experiences the smallest and largest drag forces when $W = 40$ kg/m and $W = 70$ kg/m, respectively, when $U > 0.3$ m/s. In contrast, larger weights induce minor impact on the resulting drag force exerted on the circular fish cage.

The cultivation volume of both models decreases with larger current velocities. When $U < 0.4$ m/s, the circular cage has a larger cultivation volume than the squared cage for the same dimensions and weight. The discrepancy between the cultivation volume of the two models is reduced for large velocities. Given the same dimensions, the squared fish cage has a smaller area of netting than the circular cage. Consequently, the squared cage has a larger cultivation volume and volume factor per area of netting than the circular cage. Larger weights have minor impact on the cultivation volume for both cages. The optimal way to increase the cultivation volume is by increasing the fish cage circumference. In addition, the smallest design heights result in the greatest volume factors for both fish cages. When the fish cages have the same dimensions, weight and are subjected the same velocity, the squared fish cage has a larger volume factor than the circular cage.

When the current velocity is increased, the fish cage height is reduced for most cases. The circular cage possesses a larger fish cage height than the squared cage when $U < 0.4$ m/s, given the same dimensions and weights.

Typically, the circular cage contains a larger cross-section area than the squared cage, where an increase of the current velocity results in a reduced cross-section area. The circular fish cage contains a greater cross-section area than the squared cage when $U < 0.5$ m/s, given the same dimensions and weight. In general, the different weights applied to the fish cages induce a different cross-section area, where the largest weight results in the greatest cross-section area for both cages.

The numerical results indicate that squared fish cages are superior to circular fish cages, regarding cage deformation, volume factor, cultivation volume per netting area and volume factor per netting area, given the same dimensions, weight and current velocity.

5.2. Future work

In this study, only two fish cage models with the same weight system are studied due to limit of time. Fish cages with different shapes (*e.g.*, conical shape, spherical shape and rectangular shape) and weight systems (*e.g.*, sinker tubes and single weight) can be considered in future research.

In reality, a fish farm consists of several fish cages which are aligned in arrays. In order to simulate a whole fish farm, the fish cage model needs to be integrated with a mooring system model. In addition, the interactions between cages can be investigated in the future, in order to accurately simulate the fish farm.

There are limitations with Code_Aster, especially with reaching convergence of small fish cages (small dimensions). In order to simulate small fish cages, additional convergence studies of the time interval are needed to present adequate results. Moreover, a wave module can be developed in the future for simulating aquacultural structures under a combined exposure of current and wave.

The FE solver, Code_Aster, is still in its start-up stage for dynamic analyses of fish cages. Considerable works need to be done in the future to improve the scalability, maintainability, efficiency and accuracy of the code.

6. References

ANTONUTTI, R., PEYRARD, C., INCECIK, A., INGRAM, D. & JOHANNING, L. 2018. Dynamic mooring simulation with Code_Aster with application to a floating wind turbine. *Ocean Engineering,* 151**,** 366-377.

BALASH, C., COLBOURNE, B., BOSE, N. & RAMAN-NAIR, W. 2009. Aquaculture net drag force and added mass. *Aquacultural Engineering,* 41**,** 14-21.

BI, C.-W. & XU, T.-J. 2018. Numerical study on the flow field around a fish farm in tidal current. *Turkish Journal of Fisheries and Aquatic Sciences,* 18**,** 705-716.

BI, C.-W., ZHAO, Y.-P., DONG, G.-H., XU, T.-J. & GUI, F.-K. 2014. Numerical simulation of the interaction between flow and flexible nets. *Journal of Fluids and Structures,* 45**,** 180-201.

BJØRKAN, M. & EILERTSEN, S. M. 2020. Local perceptions of aquaculture: A case study on legitimacy from northern Norway. *Ocean & Coastal Management,* 195**,** 105276.

CARDIA, F. & LOVATELLI, A. 2015. *Aquaculture operations in floating HDPE cages: a field handbook*, Food and Agriculture Organization of the United States.

CHEN, D., WANG, C. & ZHANG, H. 2021. Examination of net volume reduction of gravity-type open-net fish cages under sea currents. *Aquacultural Engineering,* 92**,** 102128.

CHEN, H. & CHRISTENSEN, E. D. 2016. Investigations on the porous resistance coefficients for fishing net structures. *Journal of Fluids and Structures,* 65**,** 76-107.

CHENG, H., LI, L., AARSÆTHER, K. G. & ONG, M. C. 2020a. Typical hydrodynamic models for aquaculture nets: A comparative study under pure current conditions. *Aquacultural Engineering***,** 102070.

CHENG, H., AARSÆTHER, K. G., LI, L. & ONG, M. C. 2020b. Numerical study of a single-point mooring gravity fish cage with different deformation-suppression methods. *Journal of Offshore Mechanics and Arctic Engineering,* 142.

DE FRANCE, E. 1989. Finite element code_aster, analysis of structures and thermomechanics for studies and research. *Open source on www. code-aster. org,* 2017.

DECEW, J., FREDRIKSSON, D., LADER, P., CHAMBERS, M., HOWELL, W., OSIENKI, M., CELIKKOL, B., FRANK, K. & HØY, E. 2013. Field measurements of cage deformation using acoustic sensors. *Aquacultural engineering,* 57**,** 114-125.

DECEW, J., TSUKROV, I., RISSO, A., SWIFT, M. & CELIKKOL, B. 2010. Modeling of dynamic behavior of a single-point moored submersible fish cage under currents. *Aquacultural Engineering,* 43**,** 38-45.

EGERSUNDNET. 2020. User manual Nets. Revision 7. Available: https://www.egersundnet.no/Egersund%20Net/Brukerh%C3%A5ndb%C3%B8ker/User%20manual%20Nets%20-%20revision%207,%20May%202020.pdf. Accessed on: 11.06.21.

ENDRESEN, P. C. & KLEBERT, P. 2020. Loads and response on flexible conical and cylindrical fish cages: A numerical and experimental study based on full-scale values. *Ocean Engineering,* 216**,** 107672.

FÉVOTTE, F. & LATHUILIÈRE, B. Studying the numerical quality of an industrial computing code: A case study on Code_aster. International Workshop on Numerical Software Verification, 2017. Springer, 61-80.

FØRE, H. M. & THORVALDSEN, T. 2021. Causal analysis of escape of Atlantic salmon and rainbow trout from Norwegian fish farms during 2010–2018. *Aquaculture,* 532**,** 736002.

FØRE, M., FRANK, K., NORTON, T., SVENDSEN, E., ALFREDSEN, J. A., DEMPSTER, T., EGUIRAUN, H., WATSON, W., STAHL, A. & SUNDE, L. M. 2018. Precision fish farming: A new framework to improve production in aquaculture. *biosystems engineering,* 173**,** 176-193.

HILBER, H. M., HUGHES, T. J. & TAYLOR, R. L. 1977. Improved numerical dissipation for time integration algorithms in structural dynamics. *Earthquake Engineering & Structural Dynamics,* 5**,** 283-292.

HUANG, C.-C., TANG, H.-J. & LIU, J.-Y. 2006. Dynamical analysis of net cage structures for marine aquaculture: Numerical simulation and model testing. *Aquacultural Engineering,* 35**,** 258-270.

HUANG, X.-H., GUO, G.-X., TAO, Q.-Y., HU, Y., LIU, H.-Y., WANG, S.-M. & HAO, S.-H. 2016. Numerical simulation of deformations and forces of a floating fish cage collar in waves. *Aquacultural Engineering,* 74**,** 111-119.

KLEBERT, P., LADER, P., GANSEL, L. & OPPEDAL, F. 2013. Hydrodynamic interactions on net panel and aquaculture fish cages: A review. *Ocean Engineering,* 58**,** 260-274.

KRISTIANSEN, T. & FALTINSEN, O. M. 2012. Modelling of current loads on aquaculture net cages. *Journal of Fluids and Structures,* 34**,** 218-235.

LADER, P., ENERHAUG, B., FREDHEIM, A., KLEBERT, P. & PETTERSEN, B. 2014. Forces on a cruciform/sphere structure in uniform current. *Ocean engineering,* 82**,** 180-190.

MORISON, J., JOHNSON, J. & SCHAAF, S. 1950. The force exerted by surface waves on piles. *Journal of Petroleum Technology,* 2**,** 149-154.

PATURSSON, Ø., SWIFT, M. R., TSUKROV, I., SIMONSEN, K., BALDWIN, K., FREDRIKSSON, D. W. & CELIKKOL, B. 2010. Development of a porous media model with application to flow through and around a net panel. *Ocean Engineering,* 37**,** 314-324.

PROIX, J., MIALON, P. & BOURDEIX, M. 2019. Eléments exacts de poutres droites et courbes. *Documentation de référence du Code_Aster,* 3.

QU, X., HU, F., KUMAZAWA, T., TAKEUCHI, Y., DONG, S., SHIODE, D. & TOKAI, T. 2019. Deformation and drag force of model square fish cages in a uniform flow. *Ocean Engineering,* 171**,** 619-624.

SHAINEE, M., ELLINGSEN, H., LEIRA, B. & FREDHEIM, A. 2013. Design theory in offshore fish cage designing. *Aquaculture,* 392**,** 134-141.

SOFIA, F. 2018. The State of World Fisheries and Aquaculture 2018-Meeting the sustainable development goals. *Fisheries and Aquaculture Department, Food and Agriculture Organization of the United Nations, Rome.*

STRAND, I. M. & FALTINSEN, O. M. 2020. Linear wave-induced dynamic structural stress analysis of a 2D semi-flexible closed fish cage. *Journal of Fluids and Structures,* 94**,** 102909.

TANG, H., XU, L. & HU, F. 2018. Hydrodynamic characteristics of knotted and knotless purse seine netting panels as determined in a flume tank. *PloS one,* 13**,** e0192206.

THÉRET, F. 1993. Etude de l'équilibre de surfaces reticules places dans un courant uniforme (application aux chalets)(Ph. D. Thesis). *Université de Nantes, Ecole Centrale de Nantes, France*.

TSUKROV, I., DRACH, A., DECEW, J., SWIFT, M. R. & CELIKKOL, B. 2011. Characterization of geometry and normal drag coefficients of copper nets. *Ocean Engineering,* 38**,** 1979-1988.

TSUKROV, I., EROSHKIN, O., FREDRIKSSON, D., SWIFT, M. R. & CELIKKOL, B. 2003. Finite element modeling of net panels using a consistent net element. *Ocean Engineering,* 30**,** 251-270.

XU, Z. & QIN, H. 2020. Fluid-structure interactions of cage based aquaculture: From structures to organisms. *Ocean Engineering,* 217**,** 107961.